The Vps13p–Cdc31p complex is directly required for TGN late endosome transport and TGN homotypic fusion

Mithu De,[1] Austin N. Oleskie,[1,3] Mariam Ayyash,[1] Somnath Dutta,[1,3] Liliya Mancour,[1,3] Mohamed E. Abazeed,[1,2] Eddy J. Brace,[1] Georgios Skiniotis,[1,3] and Robert S. Fuller[1]

[1]Department of Biological Chemistry and [2]Medical Scientist Training Program, University of Michigan Medical School, Ann Arbor, MI 48109
[3]Life Sciences Institute, University of Michigan, Ann Arbor, MI 48109

Yeast *VPS13* is the founding member of a eukaryotic gene family of growing interest in cell biology and medicine. Mutations in three of four human *VPS13* genes cause autosomal recessive neurodegenerative or neurodevelopmental disease, making yeast Vps13p an important structural and functional model. Using cell-free reconstitution with purified Vps13p, we show that Vps13p is directly required both for transport from the trans-Golgi network (TGN) to the late endosome/prevacuolar compartment (PVC) and for TGN homotypic fusion. Vps13p must be in complex with the small calcium-binding protein Cdc31p to be active. Single-particle electron microscopic analysis of negatively stained Vps13p indicates that this 358-kD protein is folded into a compact rod-shaped density (20 × 4 nm) with a loop structure at one end with a circular opening ∼6 nm in diameter. Vps13p exhibits ATP-stimulated binding to yeast membranes and specific interactions with phosphatidic acid and phosphorylated forms of phosphatidyl inositol at least in part through the binding affinities of conserved N- and C-terminal domains.

Introduction

Members of the *VPS13* gene family are conserved in all kingdoms of the Eukaryota and encode high molecular weight (3,000 to >4,000 amino acids) proteins that contain conserved domains, including N- and C-terminal domains and a domain of unknown function (Duf1162), that are not found in other proteins (Brickner and Fuller, 1997; Velayos-Baeza et al., 2004). Humans contain four full-length homologues, *VPS13A*, *B*, *C*, and *D* (Velayos-Baeza et al., 2004). A novel syntaxin 6–interacting protein, SHIP164, shares significant homology in the N-terminal domain with Vps13p (Otto et al., 2010). Atg2 proteins, essential for initiation of autophagy in eukaryotes, are reported to have both N- and C-terminal homology with Vps13 proteins based on a BLAST search–based CLANS cluster analysis (Pfisterer et al., 2014).

VPS13A is the locus for the autosomal recessive Huntington's-like neurodegenerative disease chorea acanthocytosis (Danek and Walker, 2005). Chorea acanthocytosis patients exhibit a movement disorder caused by loss of striatal neurons of the basal ganglia beginning typically in the third decade of life and progressing over 10–15 yr to death. Patients also exhibit elevated levels of aberrant red blood cells, termed acanthocytes, a property shared with two other Huntington's-like diseases, McCleod's syndrome and Huntington's disease–like-2. *VPS13B* is the locus for the autosomal recessive, craniofacial/neurodevelopmental disease, Cohen syndrome, a serious but nonprogressive disorder (Balikova et al., 2009). Genome-level genetic screens have implicated *VPS13C* as a factor in late-onset Alzheimer's disease and type II diabetes (Strawbridge et al., 2011; Meda et al., 2012). More recently, autosomal recessive loss-of-function mutations in *VPS13C* have been shown to result in a Parkinson's-like syndrome (Lesage et al., 2016). Thus, although all three proteins are widely expressed, mutations appear to result in distinctive phenotypes, suggesting the evolution of divergent, but perhaps related, functions.

Budding yeast *VPS13* was first identified as *VPT2* through a selection for mutants defective in sorting of carboxypeptidase Y (CPY) to the vacuole (Bankaitis et al., 1986). Loss-of-function alleles of *VPS13*, termed *soi1* mutations, were also identified in a screen for suppressors of a mutation in the late endosome/prevacuolar compartment (PVC)–to-Golgi retrieval

Correspondence to Robert S. Fuller: bfuller@umich.edu

Abbreviations used: CB, column buffer; CPY, carboxypeptidase Y; C-tail, cytosolic tail; LPA, lysophosphatidic acid; MSS, medium-speed supernatant; PA, phosphatidic acid; PC, phosphatidyl choline; PE, phosphatidyl ethanolamine; PI, phosphatidylinositol; PI(3)P, phosphatidyl inositol-3-phosphate; PI(4)P, phosphatidyl inositol-4-phosphate; PI(5)P, phosphatidyl inositol-5-phosphate; $PI(3,4)P_2$, phosphatidyl inositol-3,4-bisphosphate; $PI(3,5)P_2$, phosphatidyl inositol-3,5-bisphosphate; $PI(4,5)P_2$, phosphatidyl inositol-4,5-bisphosphate; PIP, phosphatidyl inositol-phosphate; PVC, prevacuolar compartment; TAP, tandem affinity purification; TEV, tobacco etch virus; WT, wild type.

© 2017 De et al. This article is distributed under the terms of an Attribution–Noncommercial–Share Alike–No Mirror Sites license for the first six months after the publication date (see http://www.rupress.org/terms/). After six months it is available under a Creative Commons License (Attribution–Noncommercial–Share Alike 4.0 International license, as described at https://creativecommons.org/licenses/by-nc-sa/4.0/).

The Rockefeller University Press $30.00
J. Cell Biol. Vol. 216 No. 2 425–439
https://doi.org/10.1083/jcb.201606078

THE JOURNAL OF CELL BIOLOGY

Downloaded from http://rupress.org/jcb/article-pdf/216/2/425/1597488/jcb_201606078.pdf by guest on 08 February 2026

signal TLS1 in the Kex2p cytosolic tail (C-tail; Redding et al., 1996; Brickner and Fuller, 1997). However, these *vps13* mutations also blocked retrieval of the vacuolar protein sorting receptor Vps10p and the transmembrane peptidases Kex2p and Ste13p from the PVC to the Golgi (Brickner and Fuller, 1997). These observations presented a dilemma in that loss of a factor required for PVC-to-Golgi retrieval suppressed mutation of a signal also required for retrieval. This puzzling observation was resolved when it was found that *vps13* mutations potentiate the function of a second TGN localization signal, TLS2, in the Kex2p C-tail that delays delivery of Kex2p from the TGN to the PVC, although the mechanism for this suppression remained unknown (Brickner and Fuller, 1997).

Loss of function of *VPS13* also results in a severe sporulation defect that was used to clone the gene by complementation (Brickner and Fuller, 1997). More recently, it was found that *vps13* mutants are defective for prospore membrane closure and exhibit altered regulation of phosphatidyl inositol-4-phosphate (PI(4)P) and phosphatidyl inositol-4,5-bisphosphate ((PI(4,5)P_2)) on the prospore membrane (Park and Neiman, 2012). Vps13p is a 3,144-aa (358-kD) peripheral membrane protein that is found in a soluble, slowly sedimenting pool; a membrane-associated pool; and a rapidly sedimenting, detergent-resistant pool (Brickner and Fuller, 1997). Proteomic analysis identified yeast centrin, Cdc31p, as a potential Vps13p-interacting protein (Kilmartin, 2003). Using a well-characterized cell-free assays for Gga2p/clathrin-dependent transport from the TGN to the PVC (Blanchette et al., 2004; Abazeed et al., 2005; Abazeed and Fuller, 2008; De et al., 2013) and for TGN homotypic fusion (Brickner et al., 2001), we now show that a purified Vps13p–Cdc31p complex is required directly for both of these processes. Purified Vps13p binds to yeast membranes in an ATP-stimulated fashion and exhibits strong, specific interactions with phosphatidic acid (PA), PI(4,5)P_2, and PI(4)P that can in part be attributed to binding specific binding sites within the conserved N- and C-terminal domains. Electron microscopic 3D reconstructions of purified monomeric protein reveal that Vps13p assumes an unusual architecture consisting of an elongated "handle" connected to a circular "loop" region.

Results

*vps13*Δ mutant extracts are defective for both TGN–PVC transport and TGN homotypic fusion

To determine whether Vps13p is required directly for TGN–PVC transport, cell-free TGN–PVC transport reactions (Fig. 1 A) were performed with medium-speed supernatant (MSS) from semi-intact cells containing donor (TGN) or acceptor (PVC) membranes from *VPS13*$^+$ and *vps13Δ* cells. Donor membranes contained either wild-type (WT) Kex2p or a chimera, K-V, in which the Vps10p C-tail replaces that of Kex2p (Abazeed and Fuller, 2008). Acceptor PVC membranes contained the PSHA (Pep12-Ste13-αF-3xHA chimera) reporter (Blanchette et al., 2004). Delivery of Kex2 activity (K-V or Kex2p) from donor membranes to acceptor membranes results in cleavage of the reporter protein, PSHA, which is monitored by measuring the fraction of DPAPase activity remaining in the supernatant after immunoprecipitation ("fraction of PSHA processed"; Fig. 1 A). As seen previously (Abazeed and Fuller, 2008), on incubating *VPS13*$^+$ donor and acceptor MSS with K-V in the donor membranes, the reaction proceeds after a lag of ∼7.5 min (Fig. 1 B, black triangles). With Kex2p in the donor membranes, the reaction exhibits slightly different kinetics (Fig. S1 A, black triangles) caused by the presence of an early, Gga2-independent phase (Abazeed and Fuller, 2008; see Materials and methods for further explanation of the differences in assays with Kex2p and K-V donor membranes). With *vps13Δ* donor and acceptor MSS, no cleavage of PSHA occurred upon incubation for 20 min with either K-V or Kex2p in the donor membranes (Figs. 1 B and S1 A, blue circles). Likewise, with *VPS13*$^+$ donor containing K-V and *vps13Δ* acceptor, no net cleavage of PSHA was seen during the 20-min incubation (Fig. 1 B, green squares). With *VPS13*$^+$ donor containing Kex2p and *vps13Δ* acceptor, a slight increase was seen in the first 7.5 min, suggesting that the early Gga-independent phase is Vps13p independent (Fig. S1 A, green squares). In contrast, when donor MSS (K-V or Kex2p) was from *vps13Δ* cells and acceptor MSS was from *VPS13*$^+$ cells, a significant increase in PSHA cleavage was seen over the entire 20-min time course (Figs. 1 B and S1 A, red diamonds). These results indicate that direct, Gga-dependent TGN–PVC transport is completely defective when both donor and acceptor MSSs lack Vps13p or when acceptor membranes alone lack Vps13p. However, a partial reaction can occur when acceptor membranes contained Vps13p, indicating a crucial role for Vps13p at the PVC in TGN–PVC transport.

The requirement for Vps13p in TGN homotypic fusion was also tested using a cell-free assay (Brickner et al., 2001). In this assay, the SHA (Ste13-αF-3xHA chimera) reporter is localized to the TGN by determinants in the Ste13p C-tail (Fig. 1 C). In control reactions (*VPS13*$^+$ donor and acceptor), efficient processing of SHA proceeded linearly, without a lag, for 20 min with both K-V–containing and Kex2p-containing MSS (Figs. 1 D and S1 B, black triangles). Lack of Vps13p in both donor and acceptor membranes resulted in complete absence of TGN homotypic fusion (Figs. 1 D and S1 B, blue circles). In contrast to the results with the TGN-PVC reaction, lack of Vps13p in either donor or acceptor membranes alone also resulted in complete absence of a reaction (Figs. 1 D and S1 B, red diamonds and green squares). These results suggest that Vps13p must be associated with both donor and acceptor TGN membranes for TGN homotypic fusion to occur.

Addition of a source of WT Vps13p restores TGN–PVC transport to reactions using *vps13*Δ MSS

PSHA processing was restored when TGN–PVC reactions performed with donor and acceptor MSS from *vps13*Δ cells were supplemented with MSS from *VPS13*$^+$ cells, but not in controls supplemented with buffer or MSS from *vps13*Δ cells (compare columns 2 and 4 to 1 and 3 in Fig. S2, A and B). MSS from cells overexpressing 3xHA-tagged Vps13p from the *ADH1* promoter exhibited greater stimulation than MSS from *VPS13*$^+$ cells (compare column 5 to columns 2 and 4 in Fig. S2, A and B). MSS from cells expressing C-terminally tandem affinity purification (TAP)–tagged Vps13p also complemented reactions conducted using MSS from *vps13*Δ cells, but complementation was lost if the Vps13-TAP MSS was first affinity-depleted using IgG Sepharose (columns 6 and 7 in Fig. S2, A and B). When samples from differential centrifugation of MSS from cells expressing C-terminally TAP-tagged Vps13p were examined by SDS-PAGE and Western blotting with anti-TAP tag antibody, a band consistent with the

Downloaded from http://rupress.org/jcb/article-pdf/216/2/425/1597488/jcb_201606078.pdf by guest on 08 February 2026

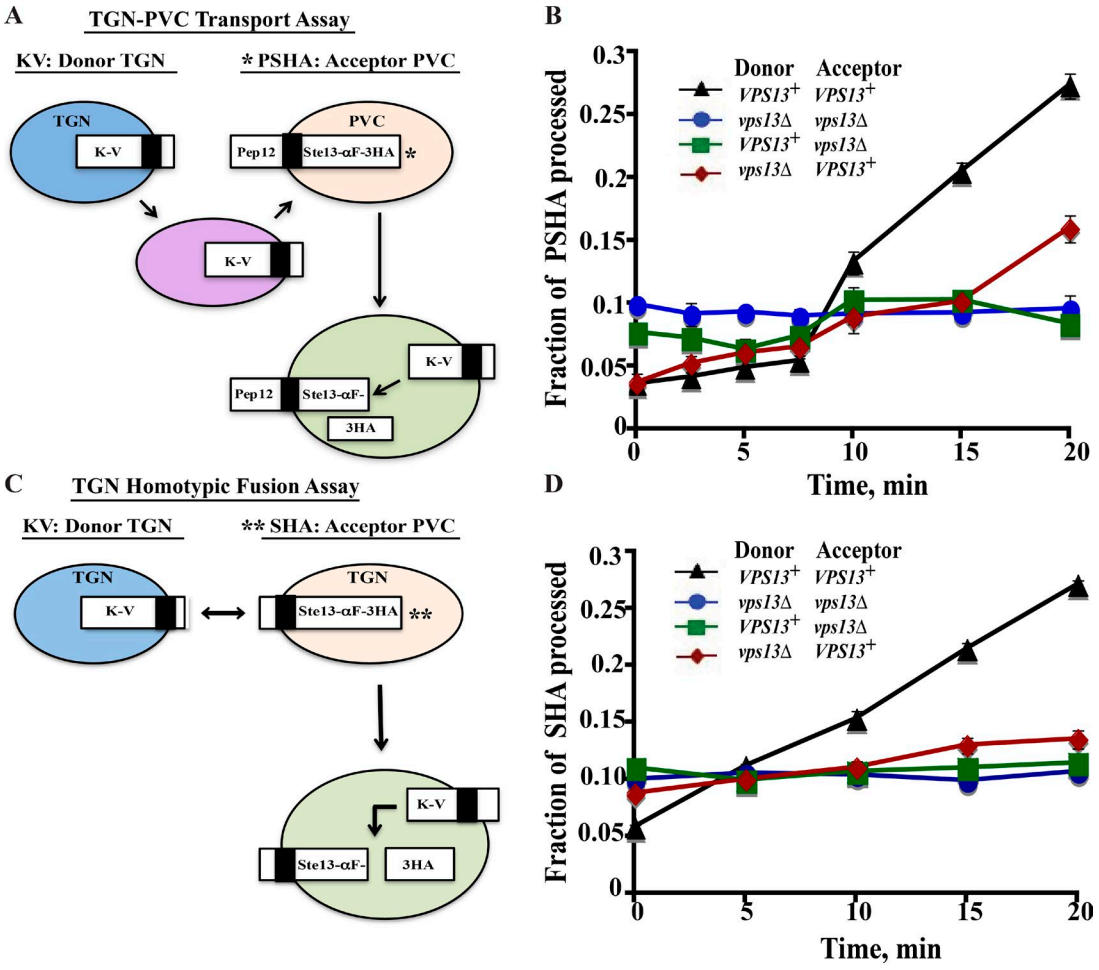

Figure 1. **MSS from *vps13*Δ cells is inactive for TGN–PVC transport and TGN homotypic fusion.** (A) Diagram of the cell-free TGN–PVC transport reaction. (B) TGN–PVC transport reactions using K-V donor MSS and PSHA acceptor MSS from *VPS13*+ and *vps13*Δ strains. Black triangles, *VPS13*+ donor and acceptor; blue circles, *vps13*Δ donor and acceptor; green squares, *VPS13*+ donor and *vps13*Δ acceptor; red diamonds, *vps13*Δ donor and *VPS13*+ acceptor. (C) Diagram of the cell-free TGN-homotypic fusion reaction. (D) TGN homotypic fusion reactions using K-V donor MSS and SHA acceptor MSS from *VPS13*+ and *vps13*Δ strains. Black triangles, *VPS13*+ donor and acceptor; blue circles, *vps13*Δ donor and acceptor; green squares, *VPS13*+ donor and *vps13*Δ acceptor; red diamonds, *vps13*Δ donor and *VPS13*+ acceptor.

expected size for Vps13-TAP (~380 kD = 358 kD (Vps13p) + 21 kD (TAP tag)) was detected (Fig. S2 C). After centrifugation at 200,000 *g*, 80% of the Vps13-TAP pelleted and 20% was in the soluble (supernatant) phase.

Purified, TAP-tagged Vps13p restores activity to TGN–PVC transport and TGN homotypic fusion reactions containing MSS from *vps13Δ* cells

C-terminally tagged Vps13p was purified from yeast expressing TAP-tagged Vps13p under the control of the *ADH1* promoter as described in Materials and methods. Purified protein characterized by SDS-PAGE followed by silver staining (Fig. 2 A), Western blotting using an anti-TAP tag antibody that recognizes the calmodulin-binding peptide left after tobacco etch virus (TEV) protease cleavage (Fig. 2 B) and Coomassie staining (Fig. 2 C) migrated at a position consistent with the expected M_r of 358 kD. Purified Vps13p restored activity to both TGN–PVC transport reactions and TGN homotypic fusion reactions conducted using donor and acceptor MSS from *vps13Δ* cells (Fig. 2, D and E). Titration of the purified protein resulted in saturation curves for both reactions. The time course of the TGN–PVC transport reaction reconstituted using a saturating amount of purified Vps13p combined with donor and acceptor MSS from *vps13Δ* cells exhibited the same pattern seen with reactions conducted using MSS from *VPS13*+ cells, with PSHA cleavage observed following a lag of 7.5 min (Fig. 2 F). Similarly, the time course of TGN homotypic fusion reconstituted using purified Vps13p combined with donor and acceptor MSS from *vps13Δ* cells proceeded without a lag, just like reactions conducted using MSS from *VPS13*+ cells (Fig. 2 G). By these criteria, purified, soluble Vps13p can reconstitute authentic TGN–PVC transport and TGN homotypic fusion by in vitro complementation, demonstrating that Vps13p acts directly in both reactions.

Single-particle EM analysis of Vps13p

To gain insights into the architecture of Vps13p, we visualized the purified protein by negative-stain EM and single-particle analysis. 2D class averages of Vps13p revealed an elongated rod-like density with a characteristic large loop structure on one end and a hook-like density on the opposite end (Fig. 3, A and B). The rod portion of the protein can be observed in straight or bent configurations stemming from a flexible portion in its middle. Comparison of the relative configuration of the

Downloaded from http://rupress.org/jcb/article-pdf/216/2/425/1597488/jcb_201606078.pdf by guest on 08 February 2026

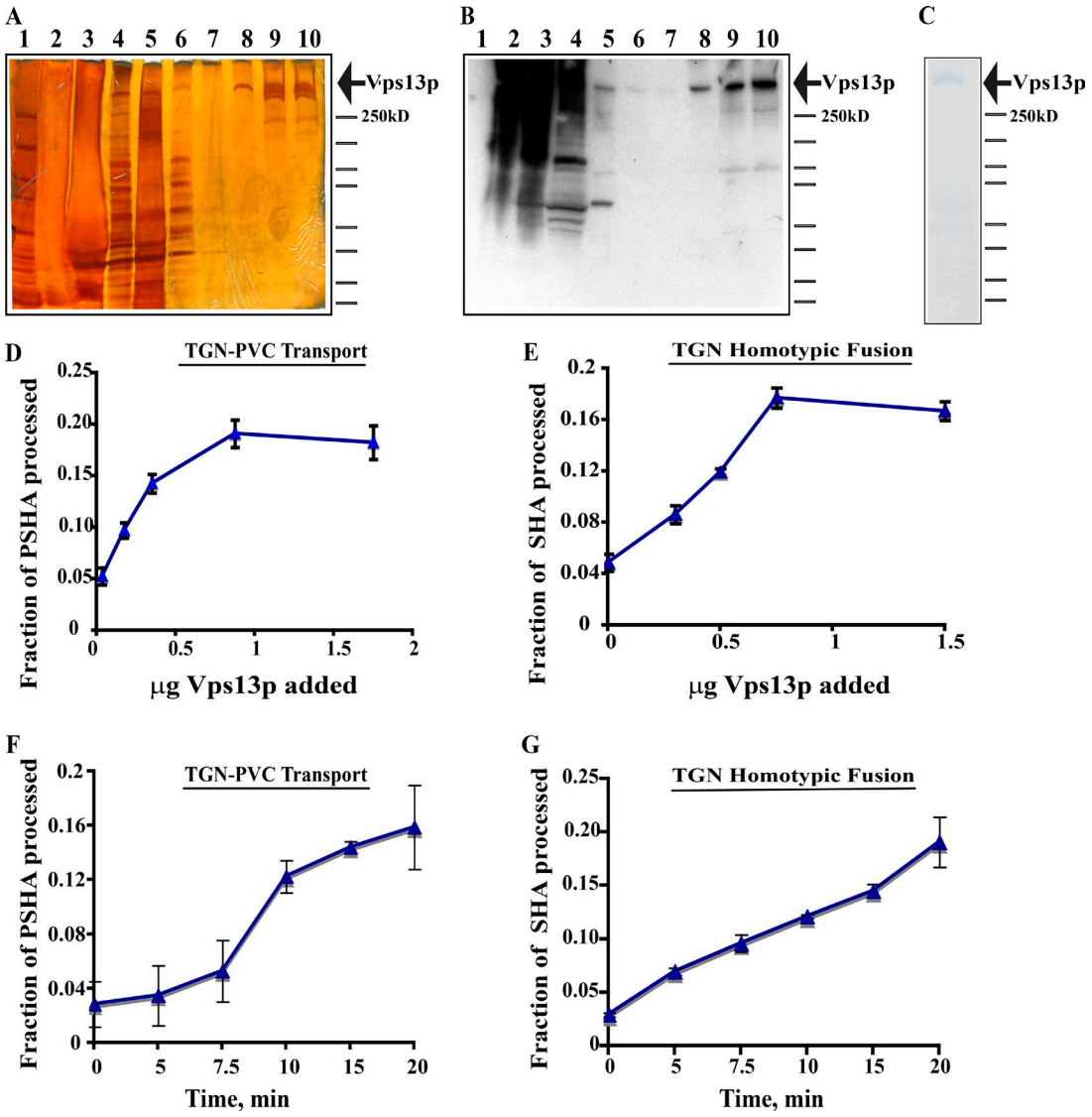

Figure 2. **Addition of purified Vps13p rescues cell-free TGN–PVC transport and TGN homotypic fusion reactions performed with *vps13*Δ extracts.** Silver-stained SDS-PAGE (A) and anti-TAP immunoblot (B) after SDS-PAGE of fractions from Vps13p purification. Lane 1, markers, lane 2, S13; lane 3, S55; lane 4, IgG Sepharose flow through; lane 5, eluate after TEV cleavage; lane 6, calmodulin Sepharose flow-through; lanes 7–10, calmodulin Sepharose eluate fractions 2–5. (C) Calmodulin Sepharose fraction 3 was analyzed by Coomassie staining after SDS-PAGE. (D) Purified Vps13p was titrated into TGN–PVC transport reactions using K-V donor MSS and PSHA acceptor MSS from *vps13*Δ strains. (E) Purified Vps13p was titrated into TGN–TGN homotypic fusion reactions using K-V donor MSS and SHA acceptor MSS from *vps13*Δ strains. (F) Time course of the TGN–PVC transport reaction using K-V donor MSS and PSHA acceptor MSS from *vps13*Δ strains. Each time point contained 1 µg purified Vps13p. (G) Time course of the TGN-homotypic fusion reaction using K-V donor MSS and SHA acceptor MSS from *vps13*Δ strains. Each time point contained 0.75 µg purified Vps13p.

diametrically opposite loop and hook regions in several class averages indicates that the middle of the rod may in fact undergo large-scale rotations. These observations were confirmed by low-resolution 3D reconstructions of distinct classes representing straight or bend protein configurations. The rod portion measured ∼4 × 20 nm, whereas the loop structure had an internal diameter of ∼6 nm.

Purified Vps13p is recruited to membranes in an ATP-stimulated fashion and exhibits specific binding to PA and phosphorylated forms of PI

Active Vps13p was purified as a soluble protein but is likely to associate with membranes to function in TGN–PVC transport and TGN homotypic fusion. To determine whether purified Vps13p became associated with membranes under reaction conditions, reactions conducted using K-V donor MSS and PSHA acceptor MSS containing purified Vps13p were fractionated using velocity sedimentation (Fig. 4 A). When the reactions were conducted in the absence of the ATP-regenerating system, 55 ± 3% of added Vps13p pelleted with membranes (Fig. 4, compare supernatant [lane 2] with pellet [lane 3]). When the reactions contained the ATP regenerating system, 90 ± 5% of the added Vps13p pelleted with membranes (Fig. 4, compare supernatant [lane 5] with pellet [lane 6]). These results suggested that binding of Vps13p to membranes involved energy-dependent and energy-independent components.

One possible mode of energy-independent membrane association would be binding to phospholipids. Binding of purified Vps13p to phospholipids was first examined using

Downloaded from http://rupress.org/jcb/article-pdf/216/2/425/1597488/jcb_201606078.pdf by guest on 08 February 2026

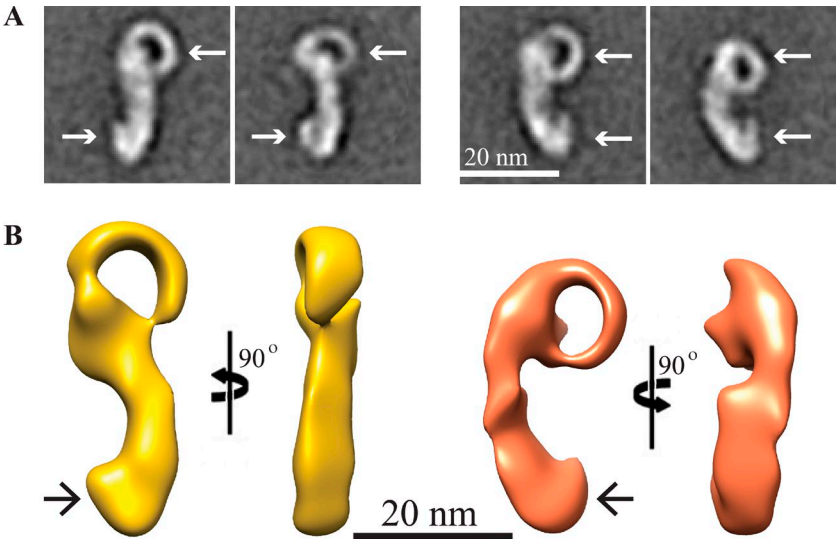

Figure 3. **3D architecture of Vps13p.** (A) 2D class averages of Vps13 reveal an elongated rod with a loop structure on one end and a hook-like density on the opposite end. The rod can be observed in straight (left) or kinked configurations (right). The loop and hook structures (indicated by arrows) can be observed on the same or opposite sides, suggesting rotational flexibility between the top and bottom half of the protein. (B) 3D reconstructions of Vps13 with the loop and hook structures on the opposite (left) or the same side (right) of Vps13. The 3D maps confirm that the loop structure is hollow.

a phosphatidyl inositol-phosphate (PIP) strip binding assay (Fig. S4 and Table S1). Purified Vps13p exhibited binding to PA and mono- and diphosphorylated phosphatidyl inositol (PI), very low binding to phosphatidyl serine (PS), and no apparent binding to lysophosphatidic acid (LPA), lysophosphatidyl choline, PI, phosphatidyl ethanolamine (PE), phosphatidyl choline (PC), sphingomyelin-1-phosphate, or phosphatidylinositol-3,4,5-tris-phosphate. On the basis of this result, binding was measured using liposome floatation assays (Fig. 4 B and Table 1). Binding of purified Vps13p was measured to 100-nm filter-extruded synthetic liposomes of the composition 50:40:10 1-palmitoyl-2-oleoyl-*sn*-glycero-3-phosphocholine/1-palmitoyl-2-oleoyl-*sn*-glycero-3-phosphoethanolamine/cholesterol (relative mole fractions) containing no addition or 5% of PA or phosphorylated forms of PI. The results of these assays largely conformed to the results of the PIP-strip assay, with Vps13p exhibiting the binding preference PA > $PI(4,5)P_2$, PI(4)P > phosphatidyl inositol-3-phosphate (PI(3)P), phosphatidyl inositol-5-phosphate (PI(5)P), LPA > phosphatidyl inositol-3,4-phosphate [$PI(3,4)P_2$], phosphatidyl inositol-3,5-bisphosphate ($PI(3,5)P_2$) > PS, PI. The ability of Vps13p to bind with significant affinity both to PA and to multiple phosphorylated forms of PI raised the question of whether these lipids bind to the same or different sites on the protein. Combinations of PA with PI(3)P or PI(4)P did not have strong synergistic effects on binding that might be expected from combinatorial binding (Table S2), but further experiments (following section) were performed to address this issue directly.

Vps13p N- and C-terminal domains contain lipid-specific binding sites

If lipid binding were of functional importance to Vps13 proteins, then sites of specific binding might reside within one or more of the conserved domains. To test this hypothesis, His_6-tagged recombinant polypeptides incorporating the conserved N- and C-terminal domains of Vps13p were expressed in *Escherichia coli* and purified (Fig. 5, A and B; Materials and methods) and used in liposome binding assays. As shown in Fig. 5 C, the Vps13 N domain exhibited strong binding to

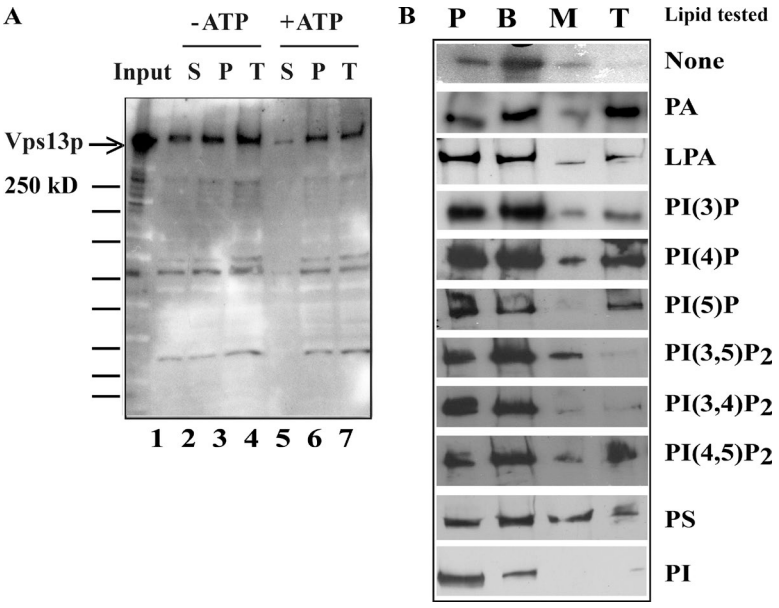

Figure 4. **Membrane and lipid binding of Vps13p.** (A) Membrane-binding reactions were conducted as described in Materials and methods. Lane 1, input (0.3 µg purified Vps13p); lanes 2–4, without ATP-regenerating system; lanes 5–7, with ATP-regenerating system, lanes 2 and 5, supernatant fractions (S); lanes 3 and 6, pellet fractions (P); lanes 4 and 7, sample of reactions before centrifugation (T). (B) Liposome-binding assays were conducted as described in Materials and methods. The figure shows data from one representative experiment. B, bottom fraction; M, middle fraction; P, pellet fraction; T, top fraction. Table 1 presents quantification of results from three independent experiments.

Downloaded from http://rupress.org/jcb/article-pdf/216/2/425/1597488/jcb_201606078.pdf by guest on 08 February 2026

Table 1. **Quantification of liposome-binding assays with full-length Vps13p**

Test lipid	Bound
	%
None	3.6 ± 1.3
PA	26.6 ± 2.5
LPA	13.7 ± 2.5
PI(3)P	17.7 ± 3.0
PI(4)P	20.0 ± 1.7
PI(5)P	15.2 ± 0.3
$PI(3,5)P_2$	6.5 ± 2.5
$PI(3,4)P_2$	7.8 ± 2.1
$PI(4,5)P_2$	20.5 ± 0.5
PS	5.8 ± 1.1
PI	2 ± 1.5

The percentage of Vps13p bound was calculated as the top fraction divided by the sum of the pellet and bottom fraction multiplied by 100. Shown are mean ± SD values from three independent experiments.

liposomes containing PA, intermediate binding to liposomes containing $PI(4,5)P_2$, and weak binding to liposomes containing PI(4)P, whereas binding to liposomes containing PI(3)P or PI(5)P was undetectable. In contrast, the C-terminal domain exhibited strong binding to $PI(4,5)P_2$-containing liposomes, but binding to liposomes containing PA, PI(3)P, PI(4)P, or PI(5)P was undetectable (Fig. 5 D). These binding data are quantified in Table 2. The purified N- and C-terminal domains exhibited dose-dependent inhibition when titrated into the TGN–PVC transport assay, suggesting that these purified lipid-binding domains interfere with the activity of endogenous Vps13p (Fig. 5 E). These results demonstrate that Vps13p contains multiple, distinct, lipid-specific binding domains. The absence of strong binding to PI(3)P or PI(4)P by these domains suggests that at least one additional lipid-binding site exists in full-length Vps13p or, alternatively, that the N and C termini have weak affinity to PI(3)P or PI(4)P on their own but exhibit a synergistic binding. The inhibition experiments support the conclusion that these domains are functionally important.

Table 2. **Quantification of liposome-binding assays with purified N and C domains of Vps13p**

Test lipid	Bound
	%
N domain	
None	2.0 ± 0.8
PA	48.0 ± 2.0
PI(4)P	19.0 ± 3.4
$PI(4,5)P_2$	31.0 ± 2.5
PI(3)P	3.0 ± 1.3
PI(5)P	2.0 ± 0.7
C domain	
None	2.0 ± 1.1
PA	6.0 ± 1.4
PI(4)P	11.0 ± 4.4
$PI(4,5)P_2$	41.0 ± 2.5
PI(3)P	8.0 ± 0.9
PI(5)P	7.0 ± 1.6

The percentage of the N domain or C domain bound was calculated as the top fraction divided by the sum of the pellet and bottom fraction multiplied by 100. Shown are mean ± SD values from three independent experiments.

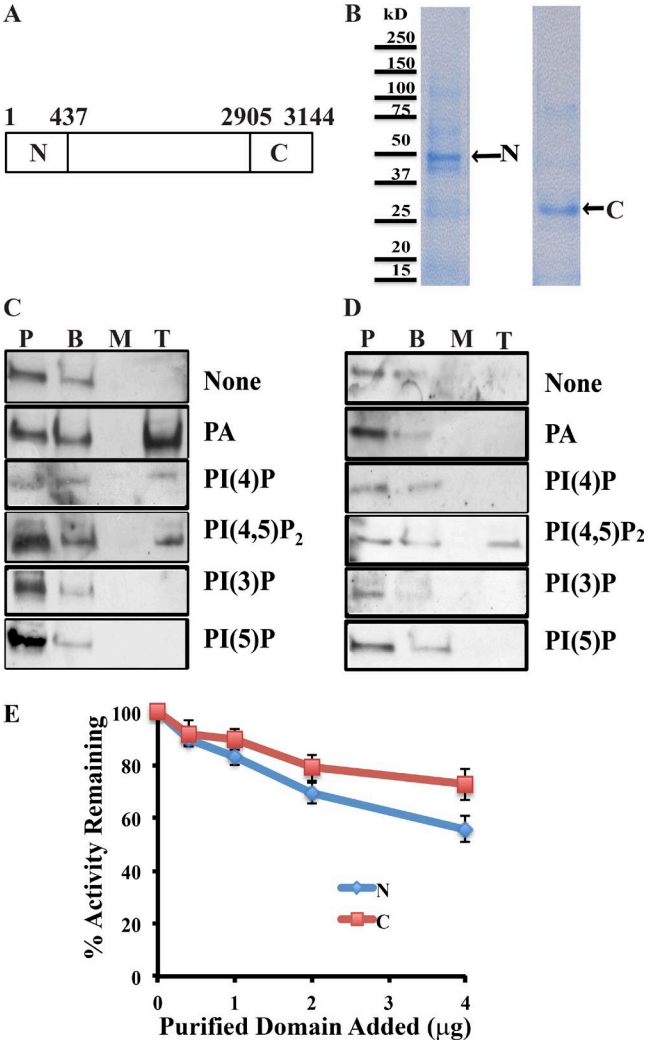

Figure 5. **Lipid binding by purified Vps13p N and C domains.** (A) Schematic representation of N domain and C domains. (B) Coomassie-stained SDS-PAGE of purified N domain (N) and C domain (C). (C and D) Liposome float-up assays were conducted as described in Materials and methods. (C) Binding assays for purified N domain. (D) Binding assays for purified C domain. The figure shows data from representative experiments. B, bottom fraction; M, middle fraction; P, pellet fraction; T, top fraction. Table 2 presents quantification of results from three independent experiments for each domain. (E) Inhibition of TGN–PVC transport by addition of purified N and C terminal domains. Purified domains were added to assembled reactions on ice before incubation at 30°C. Data are plotted as percent activity remaining and represent mean and SD of three independent experiments.

Evidence that Vps13p forms a complex with Cdc31p

Cdc31p is a calmodulin-like calcium binding protein required for spindle pole body duplication (Salisbury, 2004). A proteomic screen for proteins that interact with Cdc31p N-terminally tagged with a Z domain of protein A identified Vps13p as one of several Cdc31p-binding partners (Kilmartin, 2003). To reexamine this observation, cells containing Vps13p C-terminally fused to a triple-HA tag (Vps13-3XHA) were transformed with a ZCdc31p expression plasmid or vector control, and extracts were subjected to IgG Sepharose chromatography. A small amount of Vps13-3XHA was observed in the IgG Sepharose eluate from cells expressing ZCdc31p but was undetectable in

Downloaded from http://rupress.org/jcb/article-pdf/216/2/425/1597488/jcb_201606078.pdf by guest on 08 February 2026

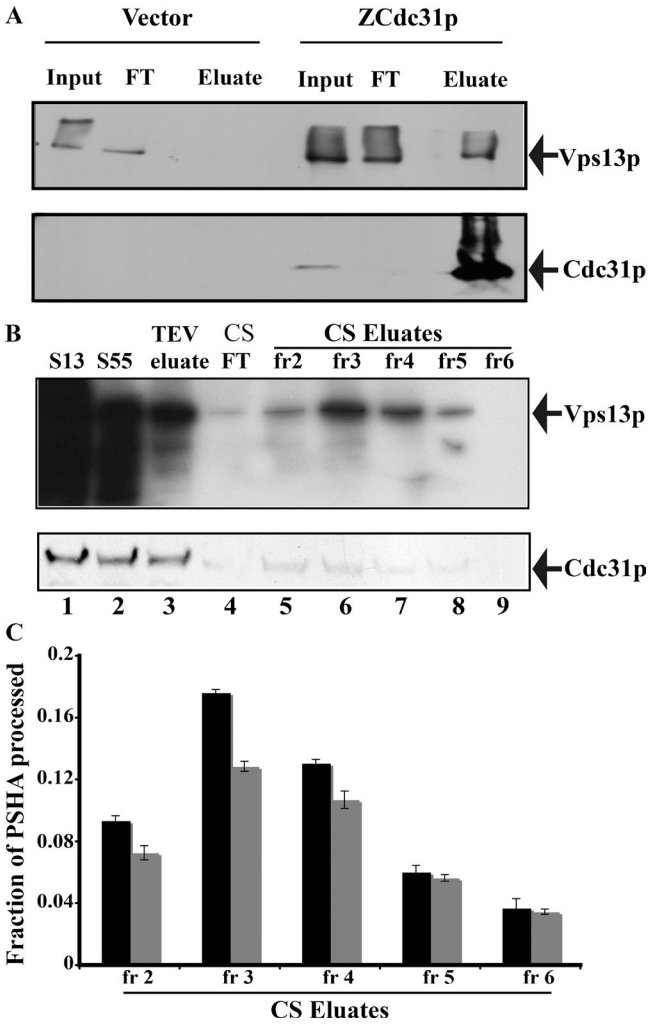

Figure 6. **Coisolation of Vps13-3XHA with Z domain–tagged Cdc31p.** (A) Experiments to measure coisolation of Vps13-3XHA with ZCdc31p were conducted as described in Materials and methods. The top blot was probed with anti–TAP antibody to detect Vps13p. The bottom blot was probed with anti–Cdc31p antibody. Eluate, IgG Sepharose eluate from cells lacking ZCdc31p (vector) or expressing ZCdc31p; FT, flow-through of IgG Sepharose; input, sample of homogenate. The input and flow-through samples represent 0.3% of the total, whereas the eluate represents 8% of the total. The ZCdc31p plasmid results in elevated expression of the 25 kD ZCdc31p relative to 18 kD endogenous Cdc31p, the latter of which is too low to be detected in samples from either the vector or ZCdc31p strains. (B) Copurification of Cdc31p with Vps13p. Fractions from Vps13p purification were immunoblotted with anti–TAP antibody to detect Vps13p (top blot) or anti–Cdc31p antibody (bottom blot). Lane 1, S13; lane 2, S55; lane 3, TEV eluate; lane 4, flow-through of calmodulin Sepharose column (CS FT); lane 5–9, eluted fractions 2–6 from calmodulin Sepharose (CS eluate). (C) Complementation by 5 μl of fractions 2–6 of calmodulin Sepharose elution shown in B of TGN–PVC transport reactions conducted with K-V donor and PSHA acceptor from *vps13*Δ strain (black columns) or *cdc31-2ts* strain (gray columns).

the eluate from vector-containing cells (Fig. 6 A), qualitatively confirming Kilmartin's result. Conversely, immunoblots of fractions from Vps13p purifications probed with anti–Cdc31p antibody showed that Cdc31p copurified with Vps13p on calmodulin Sepharose (Fig. 6 B). This activity profile of the eluate from calmodulin Sepharose for complementation of TGN–PVC transport using *vps13*Δ donor and acceptor MSS (Fig. 6 C) parallels the elution profile of the presumptive purified Vps13p–Cdc31p complex (Fig. 6 B).

Overexpression of Vps13p under *GAL1* promoter control was toxic (Fig. 7), with overexpressing cells exhibiting a terminal phenotype similar to that reported for *cdc31-ts* cells grown at the nonpermissive temperature; namely, large-budded cells in which the nucleus was restricted to the mother cell (unpublished data). Overexpression of Cdc31p rescued the poor growth phenotype of cells overexpressing Vps13p (Fig. 7), suggesting that the toxicity resulting from Vps13p overexpression was caused by sequestration of the essential protein Cdc31p.

cdc31-ts mutants extracts are defective for TGN–PVC transport, and TGN homotypic fusion and can be complemented by purified Vps13p

To determine whether Cdc31p, like Vps13p, is required for vacuolar protein sorting in vivo, a collection of *cdc31-ts* mutants was screened for temperature-sensitive secretion of CPY (Fig. S5, A–C). The mutants in this collection exhibit distinct phenotypes in spindle pole body duplication, cell morphogenesis, and integrity (Ivanovska and Rose, 2001). None of the *cdc31-ts* alleles tested exhibited substantial levels of CPY secretion at the permissive temperature (25°C). However, the tested alleles exhibited a range of effects on CPY secretion at the nonpermissive temperature (37°), with some mutants exhibiting no more CPY secretion than Vps$^+$ control strains and others exhibiting elevated CPY secretion. The strongest Vps$^-$ phenotype was exhibited by the *cdc31-2ts* strain. Therefore, this allele was crossed into the strain background used for cell-free transport and fusion assays, and the resulting strain (MDY9) was transformed with plasmids used for expression of K-V, PSHA, and SHA. MSSs from these transformants were tested for cell-free TGN–PVC transport and TGN homotypic fusion (Fig. 8, A and B). In the TGN–PVC transport assay, reactions conducted with *cdc31-2ts* donor and acceptor MSS exhibited an elevated background and were completely defective for transport (Fig. 8 A). Similar to what was seen with *vps13*Δ strains, assays conducted with *cdc31-2ts* donor but WT acceptor exhibited a partial reaction. Moreover, TGN homotypic fusion reactions conducted with *cdc31-2ts* donor and acceptor MSS in all combinations were defective (Fig. 8 B), just as had been seen with *vps13*Δ strains. Remarkably, both TGN–PVC transport and TGN homotypic fusion reactions conducted with *cdc31-2ts* donor and acceptor MSS were complemented by addition of purified Vps13p (Fig. 8, C and D). Furthermore, the presumptive Vps13p–Cdc31p complex eluted from calmodulin Sepharose exhibited comparable activity in complementation of TGN–PVC transport reactions using either *vps13*Δ or *cdc31-2ts* donor and acceptor MSS (Fig. 6 C).

Vps13p purified from a *cdc31-ts* strain cannot complement reactions conducted with MSS from either *vps13*Δ or *cdc31-ts* strains

If the active form of purified Vps13p is a Vps13p–Cdc31p complex, then Vps13p purified from a *cdc31* mutant background should be defective for complementation. Therefore, *cdc31-2ts* was crossed into the strain expressing TAP-tagged Vps13p, and Vps13p was purified from this strain (Fig. 8 G). Vps13p purified from the *cdc31-2ts* background was completely inactive for complementation of TGN–PVC transport and TGN homotypic fusion in reactions using donor and acceptor MSS from both *cdc31-2ts* (Fig. 8, C and D) and *vps13*Δ strains (Fig. 8, E and

Downloaded from http://rupress.org/jcb/article-pdf/216/2/425/1597488/jcb_201606078.pdf by guest on 08 February 2026

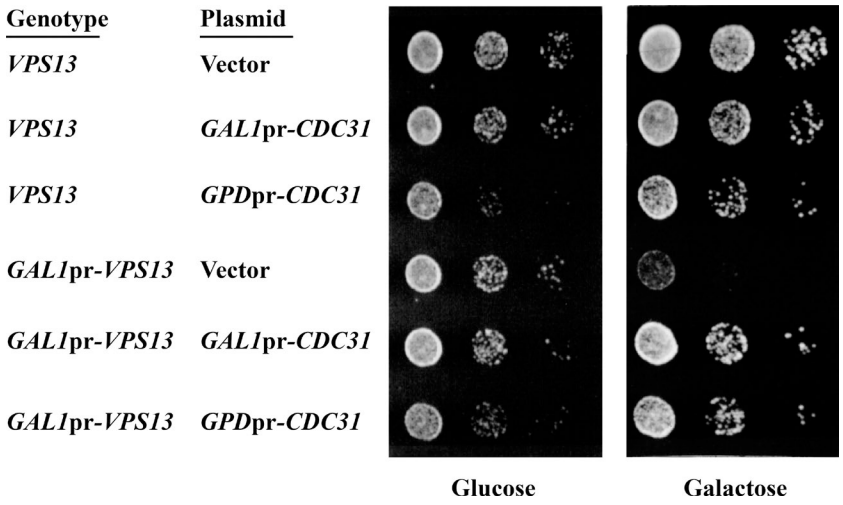

Figure 7. **Cdc31p overexpression rescues toxicity of Vps13p overexpressed under GAL1 promoter control.** pRS316 (vector), p416-*GALpr-CDC31* expressing *CDC31* under *GAL1*promoter control (*GAL1pr-CDC31*), and plasmid p426-*GPDpr-CDC31* expressing *CDC31* under *TDH3* promoter control were transformed into *VPS13*+ strain CRY1 and EBY43, in which the *GAL1* promoter was integrated in front of the *VPS13* structural gene. Strains were grown in YPD liquid culture, and serial dilutions were pronged onto 2% (wt/vol) glucose plates (synthetic complete 2% [wt/vol] glucose medium with uracil) and 2% (wt/vol) galactose plates (synthetic complete 2% [wt/vol] galactose medium with uracil) and grown for 2 d at 30°C.

F). We thus conclude that Vps13p must be in a complex with functional Cdc31p to be active and that the purified Vps13p that is active for complementation is a Vps13p–Cdc31p complex.

Discussion

Here, we demonstrate using purified Vps13p and a cell-free assay that specifically measures Gga2/clathrin-dependent transport from the TGN to the PVC that Vps13p is directly required for TGN–PVC transport. Furthermore, we find that Vps13p is required for TGN homotypic fusion. In both reactions, the active form of Vps13p is a complex of Vps13p and Cdc31p. Furthermore, we have shown that purified, soluble Vps13p is monomeric, folds into a coherent and unusual structure, and binds to yeast membranes in an ATP-stimulated fashion and that the protein has particular affinity for PA, PI(4)P, $PI(4,5)P_2$, and, to a lesser extent, other monophosphorylated phosphatidylinositides.

Membrane recruitment and lipid binding

Upon lysis, the majority of Vps13p is found in a particulate fraction (Fig. S2 C). TAP-tagged Vps13p was purified from a soluble pool, suggesting that its ability to restore TGN–PVC transport and TGN homotypic fusion to reactions conducted with extracts from *vps13*Δ cells depended on recruitment of the protein to membranes. Indeed, purified Vps13p was found to bind to membranes, and binding was stimulated by ATP. ATP stimulation may reflect a requirement for lipid or protein phosphorylation and/or an energy-dependent step. Indeed, interactions of both human VPS13B and VPS13C with rab GTPases have been reported (McCray et al., 2010; Seifert et al., 2015). The ability of purified Vps13p to associate selectively with PA and phosphorylated forms of PI suggests that direct lipid interactions are also likely to play a role in membrane recruitment. Supporting this conclusion, the conserved N- and C-terminal domains of Vps13p, expressed and purified from *E. coli*, exhibited distinct patterns of lipid-specific binding in liposome float-up assays, with the N-terminal domain exhibiting strong binding to PA, moderate binding to $PI(4,5)P_2$ and weak binding to PI(4)P, whereas the C-terminal domain bound only to $PI(4,5)P_2$. Moreover, both domains exhibited inhibitory activity when titrated into TGN–PVC transport assays. Neither domain exhibited binding to PI(3)P or PI(5)P, which did bind to full-length Vps13p, suggesting that the full-length protein contains additional binding sites. Alignments of Vps13 N-terminal domains suggest that the N-terminal domain may itself consist of two independent domains. Hypothetically, these could contain distinct binding sites for PA and $PI(4,5)P_2$.

The high affinity of Vps13p for PA, PI(4)P and $PI(4,5)P_2$ in liposome binding assays is particularly interesting in the context of the finding that *vps13* null mutations result in reduced PA, PI(4)P, and $PI(4,5)P_2$ in prospore membranes (Park and Neiman, 2012). This result suggests that there may be a complex interplay in which membrane recruitment of Vps13p results in generation of lipids that, in turn, enhance or modify Vps13p membrane association.

Additional protein–protein interactions may also be important in recruitment of Vps13p to specific membranes. For example, Spo71p is specifically required for recruitment of Vps13p to the prospore membrane during sporulation (Park et al., 2013), suggesting the possibility that specific factors are required to guide Vps13p to specific sites that would include PVC, TGN, and nuclear–vacuolar and vacuole–mitochondrial junctions (Lang et al., 2015; Park et al., 2016). SHIP164 interacts with syntaxin 6 through a domain homologous to the N-terminal conserved regions of VPS13 proteins (Otto et al., 2010). Human VPS13A extracted from erythrocyte membranes is found in complex with both β-adducin and β-actin, suggesting possible interactions of VPS13 proteins with cytoskeletal elements (Shiokawa et al., 2013).

The Vps13p–Cdc31p complex

Purified Vps13p contains Cdc31p, and the presence of Cdc31p is essential for activity in both TGN–PVC transport and TGN homotypic fusion. Moreover, temperature-sensitive alleles of *CDC31* exhibit temperature-dependent defects in CPY sorting, consistent with a role for Cdc31p in trafficking of the CPY receptor, Vps10p (Marcusson et al., 1994; Cooper and Stevens, 1996). It is conceivable that purified Vps13p contains other associated polypeptides that affect the in vitro transport and fusion reactions but, like Cdc31p, are not easily detected in silver- or Coomassie-stained gels. Likewise, we cannot absolutely rule out indirect effects of Cdc31p on Vps13p function.

Binding of Cdc31p to Vps13p could play an essential structural role, but it may also play a calcium-dependent regulatory role in Vps13 function. The crystal structure of Cdc31p bound to α-helical peptides from the spindle pole body protein

Downloaded from http://rupress.org/jcb/article-pdf/216/2/425/1597488/jcb_201606078.pdf by guest on 08 February 2026

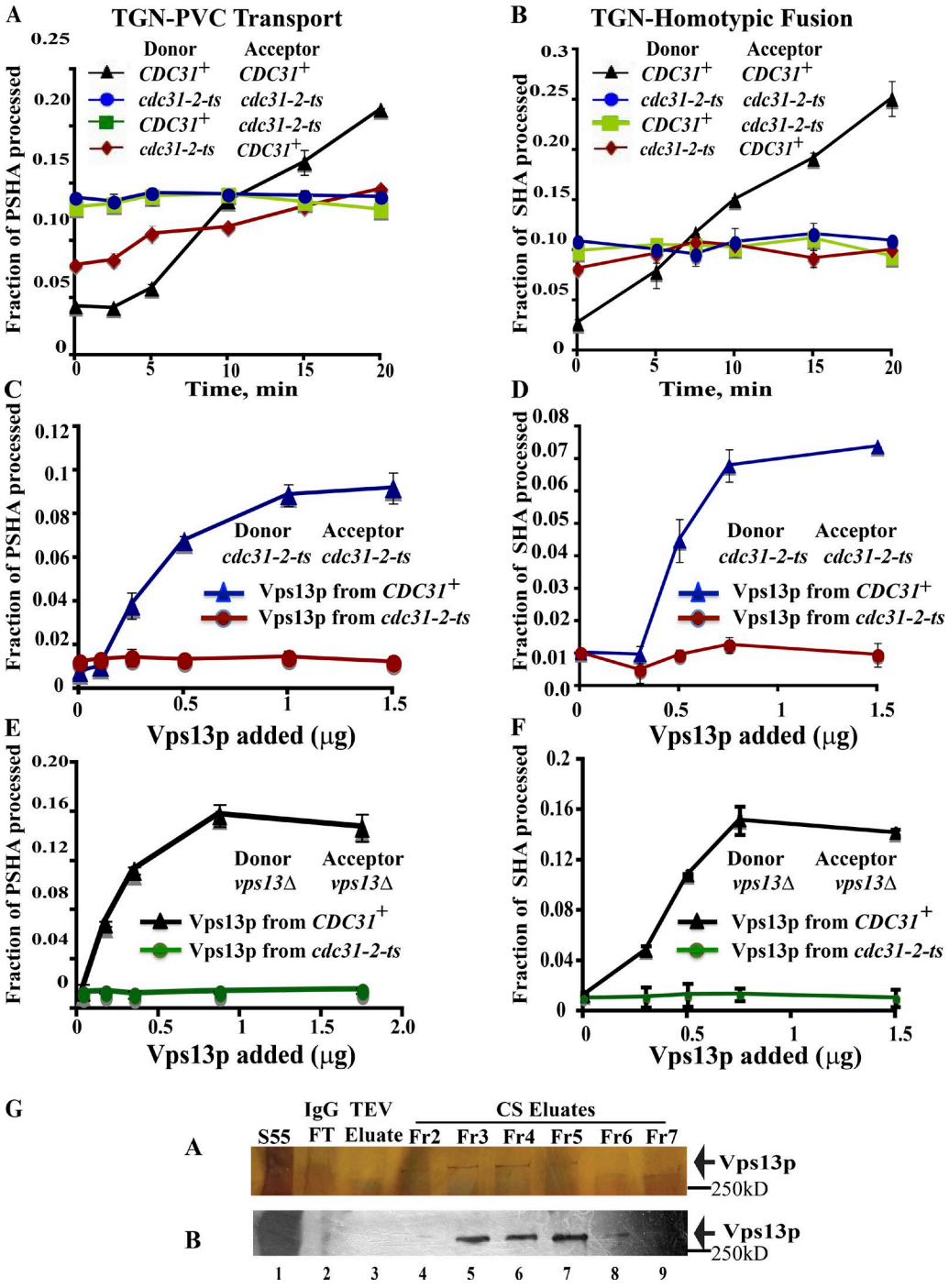

Figure 8. **Analysis of Cdc31p function using cell-free TGN–PVC and TGN homotypic fusion reactions.** (A) TGN–PVC transport reactions using K-V donor MSS and PSHA acceptor MSS from *VPS13*+ *CDC31*+ and *VPS13*+ *cdc31-2ts* strains. Black triangles, *VPS13*+ *CDC31*+ donor and acceptor; blue circles, *VPS13*+ *cdc31-2ts* donor and acceptor; green squares, *VPS13*+ *CDC31*+ donor and *VPS13*+ *cdc31-2ts* acceptor; red diamonds, *VPS13*+ *cdc31-2ts* donor and *VPS13*+ *CDC31*+ acceptor. (B) TGN-homotypic fusion reactions using K-V donor MSS and SHA acceptor MSS from *VPS13*+ *CDC31*+ and *VPS13*+ *cdc31-2ts* strains. Black triangles, *VPS13*+ *CDC31*+ donor and acceptor; blue circles, *VPS13*+ *cdc31-2ts* donor and acceptor; green squares, *VPS13*+ *CDC31*+ donor and *VPS13*+ *cdc31-2ts* acceptor; red diamonds, *VPS13*+ *cdc31-2ts* donor and *VPS13*+ *CDC31*+ acceptor. (C) Titration of Vps13p purified from *CDC31*+ strain (blue triangles) or from *cdc31-2ts* strain (red circles) into TGN–PVC transport reactions using K-V donor MSS and PSHA acceptor MSS from *VPS13*+ *cdc31-2ts* strains. (D) Titration of Vps13p purified from *CDC31*+ strain (blue triangles) or from *cdc31-2ts* strain (red circles) into TGN homotypic fusion reactions using K-V donor MSS and SHA acceptor MSS from *VPS13*+ *cdc31-2ts* strains. (E) Titration of Vps13p purified from *CDC31*+ strain (black triangles) or from *cdc31-2ts* strain (green circles) into TGN–PVC transport reactions using K-V donor MSS and PSHA acceptor MSS from *vps13Δ CDC31*+ strains. (F) Titration of Vps13p purified from *CDC31*+ strain (black triangles) or from *cdc31-2ts* strain (green circles) into TGN homotypic fusion reactions using K-V donor MSS and SHA acceptor MSS from *vps13Δ CDC31*+ strains. (G) Purification of Vps13-TAP from *cdc31-2ts* strain. Fractions from purification of Vps13-TAP from *cdc31-2ts* strain MDY9 (p416-*ADH1pr-VPS13-TAP*) were subjected to electrophoresis in SDS-PAGE and gels were silver-stained (top) or Western blotted (bottom) using anti–TAP antibody. Lane 1, S55; lane 2, IgG Sepharose flow-through (IgG FT); lane3, TEV eluate of IgG Sepharose; lane 4–9, eluted fractions 2–7 of calmodulin Sepharose (CS eluates).

Downloaded from http://rupress.org/jcb/article-pdf/216/2/425/1597488/jcb_201606078.pdf by guest on 08 February 2026

Sfi1p (Li et al., 2006) reveals interactions analogous to binding of calmodulin and myosin light chain bound to IQ-motif peptides (Trybus et al., 2007). Calcium binding by calmodulin bound to IQ motifs in myosin V causes significant conformational changes. A recent biophysical study of Cdc31p shows that Cdc31p contains one mixed, competitive Ca^{2+}/Mg^{2+}-binding site in the N terminus and two weaker Ca^{2+}-binding sites at the C terminus (Miron et al., 2011). Furthermore, the affinity of Cdc31p for a set of α-helical peptides corresponding to physiological Cdc31p-binding sites in Kar1p, Sfi1p, and Sac3p was differentially enhanced by Ca^{2+} and Mg^{2+} ions. We therefore speculate that Cdc31p may regulate Vps13p structure and function in response to changes in calcium concentrations. Indeed, cell-free TGN homotypic fusion was found to be sensitive to the rapid Ca^{2+} chelator BAPTA, but not to EGTA, suggesting a role for transient changes in Ca^{2+} levels during the reaction (Brickner et al., 2001). Localization of Vps13p to junctional complexes implicated in calcium exchange between calcium-rich organelles (vacuoles, nuclear envelope, and mitochondria) may also be relevant in this regard. The stoichiometry, sites, and possible cooperativity of binding of Cdc31p to Vps13p and the conformational effects of calcium on the Cdc31p–Vps13p complex are therefore of great interest.

Implications of the 3D structure

The EM studies reveal that Vps13p folds into a relatively compact, unitary structure that forms a complex with Cdc31p. This complex has several intriguing features that may have functional importance. The most obvious feature is the "loop" that is evident in most class averages. A second feature is the apparent flexibility of the structure in both the contour of the extended "handle" and the disposition (end-on vs. side-on) of the loop with respect to the handle. A third is the hook-like density at the end of the handle, the disposition of which relative to the loop suggests torsional flexibility in the handle. Finally, there is the appearance of one or more globular domains adjacent to the loop that may correspond to one or more of the highly conserved domains in the VPS13 family (N terminal, DUF1162, and C terminal). A major challenge will be to map both conserved domains and functional features onto this unusual structure. The loop is a particularly interesting motif. Given the apparent interaction of VPS13A with β-actin and β-adducin (Shiokawa et al., 2013), it may be worth noting that the internal diameter (∼6 nm) of the loop is similar to the diameter of an F-actin filament.

The majority of loss-of-function mutations mapped to the human *VPS13A* (chorea acanthocytosis) and *VPS13B* genes are predicted to encode truncated polypeptides, but the resulting termination codons span nearly the entire sequence of each polypeptide (Dobson-Stone et al., 2002; Seifert et al., 2009). A possible explanation for this is that the unitary, folded structures of VPS13 proteins require the integrity of the entire sequence of each protein.

Roles of Vps13 proteins in distinct types of membrane transactions

Yeast Vps13p is required for a set of distinct types of vesicular transport and fusion reactions: (a) simple homotypic fusion (TGN homotypic fusion), (b) interorganellar transport (Gga-clathrin–dependent TGN–PVC transport and retromer-dependent PVC–Golgi transport), and (c) more complex reactions (prospore membrane closure). The latter reaction is notable in that it involves not only fusion of the prospore membrane but also simultaneous scission of the nuclear envelope, a process that is topologically similar to fungal cytokinesis (Park and Neiman, 2012). Studies of VPS13 homologues in other organisms suggest an even wider portfolio of functions for these proteins that include phagosome formation, dependent on TtVPS13A in *Tetrahymena thermophila* (Samaranayake et al., 2011); Golgi ribbon fusion, dependent on VPS13B in human cells (Seifert et al., 2011); and autophagosome closure, dependent on TipC in *Dictyostelium discoideum* and VPS13A in HeLa cells (Muñoz-Braceras et al., 2015). In addition, studies in yeast have demonstrated Vps13p localization to and function in multiple interorganellar junctional complexes that include nuclear–vacuolar, vacuolar–mitochondrial, and, possibly, ER–lipid droplet junctions (Grippa et al., 2015; Lang et al., 2015; Park et al., 2016).

Even though each of the four human VPS13 homologues exhibits wide tissue expression, mutations in VPS13A to VPS13D have distinct phenotypic consequences that, presumably, reflect loss of one type of function. Understanding these diseases will require identification of the specific functional cellular defect that results from loss of each individual protein. This, in turn, requires that we understand the set of molecular functions of each of the proteins. Given the homology between all VPS13 family members, we think it is possible that there is a set of common molecular functions shared by all VPS13 homologues, in addition to unique functions. What might the common functions be? Given the evidence from this work, studies of the effects of *vps13* mutations on yeast sporulation and the involvement of Vps13p at interorganellar junctions, it seems plausible that the binding to and regulation of specific phosphorylated lipids represent common core functions. This notion is supported by recent studies on the effects of VPS13A on PI(4)P metabolism in PC12 cells (Park et al., 2015).

Finally, as shown here, Vps13p has affinity for phosphorylated lipids typically found in distinct membranes in vegetative yeast cells: PI(4)P in Golgi/TGN, $PI(4,5)P_2$ in plasma membrane, and PI(3)P in endosomal membranes. No synergistic effects on binding were found by combining PA with PI(3)P or PI(4)P, yet the properties of the purified N- and C-terminal domains suggest strongly that Vps13p contains multiple distinct lipid-specific binding sites. One attractive model that fits these data is one in which the distinct lipid-binding sites in Vps13p are topologically distinct, possibly permitting Vps13p to simultaneously bind apposed membranes that have different lipid compositions. The hypothetical ability of Vps13p to bridge distinct membrane compartments suggests a "tether-like" function for the protein, but this term may not capture the complexity of function of a molecule involved in so many distinct membrane transactions and protein interactions that may include interactions with the actin cytoskeleton (Shiokawa et al., 2013) and regulatory effects on phospholipid metabolism (Park and Neiman, 2012; Park et al., 2015). Nevertheless, this property would be consistent with roles for Vps13p both in fusion of different membrane types and in formation of interorganellar junctional complexes.

Materials and methods

Strains, plasmids, media, antibodies, and reagents

The yeast strains used in this study are listed in Table 3 and Fig. S5 C. The basic strain used for TGN–PVC transport and TGN homotypic

Downloaded from http://rupress.org/jcb/article-pdf/216/2/425/1597488/jcb_201606078.pdf by guest on 08 February 2026

fusion reactions was JBY209 (Brickner et al., 2001). A *vps13*Δ derivative of JBY209 was created by complete gene replacement using pUG72 (Gueldener et al., 2002) as a PCR template. Ura$^+$ transformants were confirmed by PCR, and *MAT*a Ura3$^-$ variant (MDY1) was selected using 5-fluoroorotic acid plates.

To construct Vps13p-tagged and overproducing strains, BY4741 containing *VPS13* with a C-terminal TAP tag (GE Healthcare) was made *pep4*$^-$ by transforming with the BamHI fragment of pTS17 and selecting for Leu$^+$ (Deloche and Schekman, 2002), generating MAY21. *VPS13-TAP* and *VPS13-3HA* were placed under control of the *ADH1* promoter by transforming MAY21 and JBY171, respectively, with a PCR fragment derived from pFA6a-kanMX6-pADH1 and selecting for G418^r (Petracek and Longtine, 2002), generating MAY22 and MAY23. A *cdc31-2ts* derivative of JBY209 (MDY9) was constructed by mating JBY209 (*MAT*a) with ELW55-2B (*MAT*α), followed by sporulation and random spore selection. To purify Vps13-TAP from a *cdc31-2ts* strain, MDY9 was transformed with p416-*ADH1pr-VPS13-TAP*. This plasmid was constructed in multiple steps from p416ADH (Mumberg et al., 1995) by inserting 500-bp fragments corresponding the 5′ end of *VPS13* and the 3′ end of *VPS13* fused by overlap extension to the TAP tag with the 5′ and 3′ fragments of *VPS13* separated by a Sma1 restriction site. This plasmid was cleaved with Sma1 and cotransformed with pSOI1.16 into JBY154-1D (Brickner and Fuller, 1997) to generate p416-*ADH1pr-VPS13-TAP* by recombination. EBY43 (*GAL1pr-VPS13*) was created by integration of the *GAL1* promoter in front of *VPS13* in strain CRY1, the *MATa* form of CRY2 (Wilcox and Fuller, 1991), by integrating the kanMX6-PGAL1 cassette from plasmid pFA6a-kanMX6-PGAL1 (Petracek and Longtine, 2002). To create strains for preparation of MSS for cell-free assays, MDY1 and MDY9 were transformed with pCW-KX10 (which encodes Kex2p; Wilcox et al., 1992), pCW-KX10-Vps10 (which encodes the Kex2-Vps10p chimera, K-V; Abazeed et al., 2005), pSHA (which encodes SHA; Brickner et al., 2001), and pPSHA (which encodes PSHA; Blanchette et al., 2004). Plasmid pRS314-ZCdc31p was a gift from J. Kilmartin (MRC Laboratory of Molecular Biology, Cambridge, England, UK; Kilmartin, 2003). Plasmids p416-*GALpr-CDC31*, expressing *CDC31* under *GAL1*promoter control (*GAL1pr-CDC31*), and p426-*GPD-pr-CDC31*, expressing *CDC31* under *TDH3* promoter control, were created by inserting a PCR fragment containing the WT *CDC31* open reading frame into plasmids p416GAL and p424GPD (Mumberg et al., 1995), respectively.

Yeast-rich medium (YPD), synthetic minimal 2% (wt/vol) glucose medium, synthetic complete 2% (wt/vol) glucose medium, synthetic complete 2% (wt/vol) galactose medium, and synthetic complete dropout media, such as synthetic complete 2% (wt/vol) glucose medium with uracil, were prepared as described previously (Rose et al., 1990). Unless otherwise specified, yeast cells were grown at 30°C. Anti–HA mAb 12CA5 was obtained from Roche. Affinity-purified rabbit anti–mouse IgG was obtained from Jackson ImmunoResearch Laboratories, Inc. Rabbit polyclonal anti–TAP antibody was obtained from GenScript. Rabbit anti–yeast Cdc31p antibody was a gift from M. Rose (Princeton University, Princeton, NJ). Rabbit anti–His_6 antibody was obtained from Bethyl Laboratories, Inc. IgG Sepharose 4B and protein A Sepharose were obtained from GE Healthcare. Pansorbin was obtained from EMD Millipore. Restriction endonucleases, DNA modification enzymes, and calf intestinal alkaline phosphatase were purchased from New England Biolabs, Inc. Ala-Pro-MCA was purchased from Bachem. PIP strips were purchased from Echelon Biosciences. Phospholipids were purchased from Avanti Polar Lipids, Inc. Precast 4–15% TGX gradient gels and Precision Plus Protein Kaleidoscope Prestained Protein Standards were purchased from Bio-Rad Laboratories. In figures, only the 250-kD standard is indicated; lines below it correspond to 150, 100, 75, 50, 37, 25, and 20 kD. All other chemicals and reagents were obtained from Sigma-Aldrich, unless otherwise indicated.

Cell-free TGN–PVC transport and TGN homotypic fusion reactions

Cell-free assays for TGN-to-PVC transport (Blanchette et al., 2004; Abazeed et al., 2005; Abazeed and Fuller, 2008; De et al., 2013) and TGN homotypic fusion (Brickner et al., 2001) were conducted as described. MSS containing TGN, endosomal membranes, and cytosol was prepared from spheroplasts of JBY209, MDY1 (*vps13*Δ), and MDY9 (*cdc31-2ts*) cells expressing Kex2p, K-V (chimera consisting of Kex2p with Vps10p C-tail), or the PSHA or SHA chimeric substrates. MDY9 (*cdc31-2ts*) cells were grown at the permissive temperature (25°C); all other strains were grown at 30°C. In brief, TGN-to-PVC transport assays measured the fractional cleavage of PSHA by Kex2p proteolytic activity delivered from K-V– or Kex2p-containing donor TGN membranes to acceptor PSHA-containing PVC membranes (Figs. 1 A and S1 A). When MSS contains Kex2p, the reaction observed with PSHA acceptor MSS (the TGN–PVC reaction) represents a composite of two reactions: a Gga-dependent reaction that shows a lag and that we interpret as authentic Gga-clathrin–dependent transport and a Gga-independent reaction that occurs early, without a lag, that most likely represents direct PVC–early endosome fusion (Abazeed and Fuller, 2008). This is consistent with the partitioning of Kex2p between two

Table 3. **Strains used in this study**

Strain	Genotype
JBY209	*MAT*α *kex2*Δ*2::hisG dap2::kan*^{r} *pep4::HIS3 ste13::LEU2*
CB018	*MATa KEX2*$^+$ *pep4::HIS3 prb1::hisG prc1::hisG*
BY4741	*MATa his3*Δ*1 leu2*Δ*0 met15*Δ*0 ura3*Δ*0*
MAY22	BY4741 *ADH1pr::VPS13*-TAP *pep4*Δ*::LEU2*
MAY23	CBO18 *ADH1pr*::VPS13-HA
DC14	*MATa his1*
ELW55-2B	*MAT*α *cdc31-2ts ura3-52 trp1*Δ
MDY1	JBY209 *vps13*Δ*::URA3*
MDY9	JBY209 *cdc31-2ts*
EBY43	*MATa ade2-1 can1-100 his3-11,15 leu2-3,-112 trp1-1 ura3-1 GAL1pr-VPS13*
JBY154-1D	*MAT*α *ade2-1 can1-100 his3-11,15 leu2-3,-112 trp1-1 ura3-1 vps13*Δ*::kan*^{r}
MS 7902	*CDC31*$^+$ *leu2-3,112 ura3-52 ade2-101 his3-*Δ*300*

JBY209 (Brickner et al., 2001), CB018 (Brenner and Fuller, 1992), BY4741 (Brachmann et al., 1998), ELW55-2B (Weiss and Winey, 1996), JBY154-1D (Brickner and Fuller, 1997), and MS 7902 (Ivanovska and Rose, 2001) were constructed as described previously. MAY22, MAY23, MDY1, MDY9, and EBY43 were constructed as described in Materials and methods.

Downloaded from http://rupress.org/jcb/article-pdf/216/2/425/1597488/jcb_201606078.pdf by guest on 08 February 2026

pathways to the PVC, one a "direct" Gga-clathrin–dependent pathway and the other a Gga-independent pathway through the early endosome (Sipos et al., 2004; De et al., 2013). With the Kex2-Vps10 chimera, K-V, in donor membranes, only the direct pathway is seen (Abazeed and Fuller, 2008), consistent with the behavior of Vps10p (Sipos et al., 2004). Thus use of K-V greatly simplifies interpretation of the assays. TGN homotypic fusion assays measured the fractional cleavage of SHA by Kex2p proteolytic activity upon fusion of donor K-V–containing or Kex2p-containing TGN membranes with acceptor SHA-containing TGN membranes (Fig. 1 C). Transport and fusion reactions were incubated at 30°C for 20 min (endpoint assays) or for the indicated times (time courses). The fraction of PSHA and SHA cleaved ("fraction of PSHA processed") was monitored by the fraction of Ste13 DPAPase activity remaining in the supernatant after anti-HA immunoprecipitation using the monoclonal anti–HA antibody 12CA5. DPAPase activity was determined using the fluorogenic substrate Ala-Pro-AMC. Data points represent mean values of triplicates; error bars represent ±SD, and all reactions presented were performed three or more times with comparable results. At least two independent preparations of MSS were tested. An elevated background was observed with *vps13*Δ and *cdc31-2ts* acceptor MSS because of Kex2-independent cleavage in vivo in mutant cells, a phenomenon observed previously with other mutations that affect sorting (Brickner et al., 2001; Abazeed et al., 2005). The elevated backgrounds imply that PSHA or SHA has been partially cleaved in vivo in a Kex2p-independent fashion in these mutant backgrounds (the PSHA and SHA "donor" strains are *kex2*-null mutants) because of subtle alterations in trafficking of PSHA or SHA or induction of altered proteolytic activities (e.g., Yps1p and Yps2p, two glycosylphosphatidylinositol-anchored aspartyl proteases, can cleave Kex2p substrates within the secretory pathway). Notably, Yps1p is induced by cell wall stress (Komano and Fuller, 1995; Krysan et al., 2005).

Purification of TAP-tagged Vps13p

Vps13-TAP–expressing strains were grown for 16 h in 2 liters of YPD at 30°C (MAY22, *VPS13-TAP*) or 25°C (*cdc31-2ts* strain MDY9 containing p416-*ADH1pr-VPS13-TAP*) to a density of 5×10^7 cells/ml, and cells were spheroplasted and frozen as described previously (Brickner et al., 2001). For purification, spheroplasts were thawed and homogenized with 10 strokes of a dounce homogenizer (pestle A), and lysates were centrifuged at 13,000 rpm for 10 min. This and subsequent steps were conducted at 4°C. The resulting MSS (also referred to as S13) was centrifuged in a TLS55 rotor in a TLX centrifuge (Beckman Coulter) at 55,000 rpm (200,000 *g*) for 1 h to generate a supernatant fraction (S55) that contained ∼20% of Vps13-TAP in a soluble form, with the remainder sedimenting with membranes or complexes (Fig. S2 C; Brickner and Fuller, 1997). 1 ml IgG Sepharose 6 Fast Flow beads (GE Healthcare), preequilibrated with TNN buffer (50 mM Tris-Hcl, pH 7.9, 50 mM NaCl, and 0.5% NP40), were added to S55 and rotated for 2.5 h. This mixture was loaded onto a 10-ml column (Bio-Rad Laboratories), flow-through was collected and the resin was washed with 3 × 10 ml TNN buffer and 2 × 10 ml TEV buffer (TNN buffer with 1 mM DTT and 0.5 mM EDTA). IgG beads were resuspended in 5 ml TEV buffer with 5 µl 1.3-mg/ml TEV protease, rotated for 16 h and loaded onto a column. TEV-cleaved Vps13p (TEV eluate) was recovered in the flow-through. The TEV eluate was rotated with 1 ml of calmodulin-Sepharose 4B beads (GE Healthcare) preequilibrated with calmodulin binding buffer (75 mM Tris-HCl, pH 7.9, 120 mM NaCl, 1 mM MgOAc, 1 mM imidazole, and 2 mM $CaCl_2$) for 2.5 h. Resin was loaded on a 10-ml column and washed with 3 × 10 ml calmodulin-binding buffer, and bound protein was eluted with 1.6 ml calmodulin elution buffer (10 mM Tris-HCl, pH 7.0, 120 mM NaCl, 1 mM MgOAc, 1 mM imidazole, and 20 mM EGTA), collected in eight 200-µl fractions. Purified fractions were stored in this buffer at −80°C. Although elution from calmodulin-Sepharose by calcium chelation may alter the calcium-binding status of Cdc31p in the Vps13p–Cdc31p complex, we think it is likely that Cdc31p remains bound. First, Cdc31p coelutes with Vps13p (Fig. 6 B). Second, Cdc31p binds with relatively high affinity to effector peptides in the absence of divalent cations. Indeed, crystal structures of Cdc31p bound to Sfi1p peptides both in the presence and absence of calcium have been reported (Li et al., 2006). To assay the activity of Vps13p during purification, TGN–PVC transport reactions were conducted using donor and acceptor MSS from *vps13*Δ cells. A unit of activity was defined as the amount of Vps13p required for cleaving 10% of the PSHA in 20 min. Protein concentrations of eluted fractions were determined by Bradford (Bio-Rad Laboratories) and BCA assays. After SDS-PAGE, purified Vps13p was visualized by Coomassie blue and silver staining. For immunoblotting gels were transferred overnight at 45 V to Protran nitrocellulose (GE Healthcare), and the blots were probed with polyclonal rabbit anti–TAP antibody and horseradish peroxidase–conjugated goat anti–rabbit IgG (Jackson ImmunoResearch Laboratories, Inc.). Blots were visualized with ECL reagents (Bio-Rad Laboratories) and HyBlot CL film (Denville Scientific), and the bands were quantified by scanning densitometry using ImageJ software (National Institutes of Health). Purified TAP-tagged Vps13p retains a C-terminal calmodulin-binding peptide that reacts with anti–TAP antibody but is referred to in this paper as Vps13p.

Membrane binding of Vps13p

To test binding of Vps13p to yeast membranes, 1.5 µg purified Vps13p was added to 90-µl reactions containing 30 µl Kex2-Vps10p donor and 30 µl PSHA acceptor MSS from *VPS13*$^+$ strain JBY209. Binding reactions were incubated for 20 min at 30°C in the presence or absence of the creatine phosphate/creatine kinase ATP-regenerating system (Brickner et al., 2001) and then centrifuged at 54,000 rpm (200,000 *g* at r_{av}) for 1 h in a TLS55 rotor (Beckman Coulter). Pellets were resuspended in 90 µl SDS-PAGE sample buffer, and one ninth each of the total reaction and the supernatant and pellet fractions was separated by SDS-PAGE and immunoblotted. The bands were quantified by scanning densitometry using ImageJ software (National Institutes of Health). Values given in Results for percentage of Vps13p in the pellet represent mean ± SD for three independent experiments.

Liposome and PIP-strip–binding assays

To prepare liposomes of defined composition, lipids were mixed at the desired molar ratio in glass containers following the method of Bigay and Antonny (2005). Control liposomes consisted of 1-palmitoyl-2-oleoyl-*sn*-glycero-3-phosphocholine:1-palmitoyl-2-oleoyl-*sn*-glycero-3-phosphoethanolamine:cholesterol in 50:40:10 wt/wt ratio. Sample liposomes consisted of control liposomes plus 5% of either PA, LPA, PI(3)P, PI(4)P, PI(5)P, PI(3,4)P_2, PI(3,5)P_2, PI(4,5)P_2, PS, or PI. All PI lipids contained 18:1 cis-9 fatty acids. Chloroform solutions of lipids were evaporated under N_2 gas and dried overnight under vacuum. The lipid films were resuspended in 250 µl liposome buffer (50 mM Hepes-KOH, pH 7.2, and 120 mM potassium acetate) and subjected to five cycles of freezing in acetone/dry ice followed by and thawing at 30°C. The multilamellar liposome suspensions were extruded 61 times through a 0.1-µM polycarbonate filter using a 250-µl Hamilton syringe to generate unilamellar liposome suspensions. 4 µg Vps13p or 2 µg recombinant N and C domains were incubated with control and sample liposomes (10 mM) in final volume of 150 µl buffer A (50 mM Hepes-KOH, pH 7.2, 120 mM potassium acetate, 1 mM $MgCl_2$, 1 mM DTT, and 10% sorbitol) for 30 min at 30°C. Protein and lipid suspensions were adjusted to 30% wt/vol sucrose by adding 100 µl of 2.2 M sucrose in buffer A and introduced beneath a step gradient

Downloaded from http://rupress.org/jcb/article-pdf/216/2/425/1597488/jcb_201606078.pdf by guest on 08 February 2026

consisting of 50 µl buffer A and 200 µl buffer A plus 0.75M sucrose in polycarbonate tubes. The tubes were centrifuged at 54,000 rpm (200,000 *g* at r_{av}) for 1 h in a TLS55 rotor. After centrifugation, three fractions were collected from bottom to top using a Hamilton syringe (bottom, 300 µl; middle, 100 µl; and top, 100 µl), and a fourth sample was prepared by resuspending pelleted material in 300 µl SDS-PAGE loading buffer. A one-tenth volume of each fraction was subjected to SDS-PAGE and immunoblotted using anti-TAP (Vps13p) or anti-His_6 (N and C domains) antibody. Blots were developed and the bands were quantified by scanning densitometry using ImageJ software.

Alignment of the *Saccharomyces cerevisiae* Vps13p N- and C-terminal regions with those of the four human homologues (VPS13A–VPS13D), two *Caenorhabditis elegans* homologues, and single homologues from *Canis lupus*, *Rattus norvegicus*, *Danio rerio*, *Pan troglodytes*, *Schizosaccharomyces pombe*, and *Dictyostelium discoideum* was done using ClustalW2 (Larkin et al., 2007). Jpred was used to better define domain boundaries (Cuff et al., 1998). Sequences encoding the N-terminal domain (codons 1–437) and C-terminal domain (codons 2905–3144) were amplified by PCR using primers listed in Table S3 and were introduced into the expression vector pMCSG7 by ligation-independent cloning. Insertion into pMCSG7 fused an N-terminal leader to each domain that contained a His_6 affinity tag (Stols et al., 2002). The resulting plasmids were transformed into BL21-DE3 *E. coli*, and expression in log-phase cultures was induced with 1 mM IPTG for 4 h at 37°C. Both polypeptides were found in inclusion bodies in sonicates of expressing cells. The N domain was solubilized with 6 M guanidinium chloride in column buffer (CB; 20 mM Tris-HCl, pH 7.9, 0.5 M NaCl, and 10% sorbitol), bound to Ni-NTA agarose (QIAGEN); renatured by sequentially washing with CB containing 3 M, 1.5 M, and 0 M guanidinium chloride; washed sequentially with CB containing 20 mM and 60 mM imidazole; and eluted with CB containing 500 mM imidazole. The C domain was solubilized with CB plus 6 M urea, bound to Ni-NTA agarose, renatured by sequentially washing with CB plus 4 M urea then CB without urea, washed sequentially with CB containing 20 mM and 40 mM imidazole, and eluted with CB containing 300 mM imidazole. Eluted proteins were dialyzed against CB.

Protein and lipid overlay assays were performed to identify lipid ligands of Vps13p by using PIP strips (Echelon Bioscience). The strip was blocked with 3% BSA in TBS (10 mM Tris-HCl, pH 7.4, and 150 mM NaCl), incubated with 3 µg purified Vps13p for 2 h at room temperature with gentle agitation and then washed with TBST (TBS + 0.1% vol/vol Tween 20). Vps13p was detected by immunoblotting with anti-TAP antibodies, the film was quantified by densitometry, and the bands were quantified by scanning densitometry using ImageJ software.

Coisolation of Vps13-3HA with ZCdc31p

Strains MAY23 and MAY23 containing pRS314-ZCdc31p were grown in 2 liters of YPD at 30°C for 16 h, and 2×10^8 cells were harvested by centrifugation and digested with lyticase as described previously (Brickner et al., 2001). Spheroplasts were washed twice with 0.7 M sorbitol, resuspended in 10 ml lysis buffer (7.5% glycerol, 50 mM Tris-Cl, pH 7.8, 0.1 M NaCl, 5 mM EGTA, 1 mM EDTA, and 1% Triton containing one EDTA-free PI tablet; Roche), and homogenized with 10 strokes of a Dounce homogenizer. The lysates were centrifuged at 13,000 rpm for 10 min at 4°C, and the supernatant fractions were removed, supplemented with 1.8 ml 1 M NaCl, and applied to 0.2-ml columns of IgG-Sepharose (GE Healthcare). The columns were washed with 20 ml wash buffer 1 (0.05% Tween 20, 150 mM NaCl, and 20 mM Tris HCl, pH 7.4) and 10 ml wash buffer 2 (5 mM NH_4Ac, pH 5.0) and eluted with 1 ml of 0.5 M acetic acid, pH 3.4. The eluates were lyophilized and resuspended in SDS-sample buffer. Samples of the homogenate, flow-through, and eluted fractions from MAY23 and MAY23 expressing ZCdc31p were subjected to SDS-PAGE and transferred to nitrocellulose, and blots were probed with anti–HA antibody (top portion to detect Vps13-3HA) or anti–Cdc31 antibody (bottom portion). For detection of ZCdc31p, transfers were conducted for 2 h at 100 V.

EM of Vps13p

TAP-tag purified Vps13p was prepared for EM by the conventional negative-staining method using 0.75% uranyl formate (Ohi et al., 2004). Imaging was performed at room temperature with a Tecnai 12 transmission electron microscope (FEI) equipped with a LaB6 filament operated at an acceleration voltage of 120 kV using low-dose procedures. 250 tilt pair images (0° and 60°) were recorded at 71,139× magnification and ∼1.4 µm defocus on a Gatan US4000 CCD camera. All images were binned (2 × 2 pixels) to obtain a pixel size of 4.16 Å at the specimen level. 14,828 particle projections were manually selected and excised using WEB (Frank et al., 1996).

The projections of the untilted particles were used for reference-free alignment and classification using ISAC (iterative stable alignment and clustering; Fig. S3; Yang et al., 2012). For 3D reconstructions, we used the random conical tilt technique (Frank et al., 1996) to calculate initial back projection maps from the tilted particle projections of two individual classes using SPIDER (system for processing of image data from electron microscopy and related fields; Frank et al., 1996). After eight iterations of refinement, untilted particle projections were added to each tilted stack, and the images were subjected to another cycle of angular refinement. Using the resulting maps filtered to 40 Å as reference model, we used RELION-1.3 (Scheres, 2012) to calculate final reconstructions of the two classes. Each final reconstruction is based on 360 projections after contrast transfer function correction. The resolution of the maps was assessed by Fourier shell correlation and estimated to be ∼30 Å.

Online supplemental material

Fig. S1 complements Fig. 1 by demonstrating that membranes from *vps13*Δ cells are defective for TGN–PVC transport and TGN homotypic fusion when donor membranes contain full-length Kex2p as opposed to the Kex2-Vps10 chimera, K-V. Fig. S2 provides evidence that MSS from WT, but not *vps13*Δ cells rescues the TGN–PVC transport defect, that overexpression of Vps13p increases the efficiency of rescue, and that affinity depletion of Vps13p eliminates rescue. Fig. S3 provides raw EM images, additional class average images, and electron micrograph analysis reconstructions of Vps13p ultrastructure. Fig. S4 presents PIP-strip binding by purified Vps13p. Fig. S5 presents analysis of the Vps phenotype of a set of temperature-sensitive mutant alleles of *CDC31*. Table S1 presents quantification of the PIP strip by Vps13p. Table S2 presents quantification of binding of Vps13p to liposomes containing mixtures of PA with PI(3)P and PI(4)P. Table S3 contains the sequences of primers used to subclone the conserved N- and C-terminal domains of Vps13p for expression in *E. coli.*

Acknowledgments

The authors thank John Kilmartin for providing the ZCdc31 plasmid and for helpful discussions, Mark Rose for providing *cdc31* mutant strains and anti–Cdc31p antibody, and Akira Ono and Balaji Olety for helpful suggestions on liposome preparation.

This work was supported by the Elyse (Lakritz) Weinbaum and Gaven Lakritz Research Fund, the Protein Folding Disease Initiative of the University of Michigan Medical School, the Advocacy for Chorea Acanthocytosis Patients, and National Institutes of Health grants

Downloaded from http://rupress.org/jcb/article-pdf/216/2/425/1597488/jcb_201606078.pdf by guest on 08 February 2026

RO1 GM50915 (to R.S. Fuller) and R01 DK090165 (to G. Skiniotis), Medical Scientist Training Program grant NIH GM0786, and Genetics Training Program grant NIH GM07544 (to M.E. Abazeed).

The authors declare no competing financial interests.

Author contributions: M. De contributed to conceptual design, conducted experiments in Figs. 1, 2, 4, 5, 6, 8, and S1, S2, S4, and S5, provided the purified protein for Fig. 3, and contributed to drafting and revising the manuscript. A.N. Oleski performed EM analysis (Figs. 3 and S3). M. Ayyash conducted experiments in Fig. 5 B. S. Dutta and L. Mancour performed analysis of EM data (Figs. 3 and Fig. S3). M.E. Abazeed contributed to conceptual design and conducted the experiment in Fig. 7 along with key preliminary experiments. E.J. Brace conducted key preliminary experiments. G. Skiniotis and R.S. Fuller contributed to conceptual design, drafting and revising the manuscript, and funding acquisition.

Submitted: 16 June 2016
Revised: 4 November 2016
Accepted: 11 January 2017

References

Abazeed, M.E., and R.S. Fuller. 2008. Yeast Golgi-localized, gamma-Ear-containing, ADP-ribosylation factor-binding proteins are but adaptor protein-1 is not required for cell-free transport of membrane proteins from the trans-Golgi network to the prevacuolar compartment. *Mol. Biol. Cell.* 19:4826–4836. http://dx.doi.org/10.1091/mbc.E07-05-0442

Abazeed, M.E., J.M. Blanchette, and R.S. Fuller. 2005. Cell-free transport from the *trans*-Golgi network to late endosome requires factors involved in formation and consumption of clathrin-coated vesicles. *J. Biol. Chem.* 280:4442–4450. http://dx.doi.org/10.1074/jbc.M412553200

Balikova, I., A.E. Lehesjoki, T.J. de Ravel, B. Thienpont, K.E. Chandler, J. Clayton-Smith, A.L. Träskelin, J.P. Fryns, and J.R. Vermeesch. 2009. Deletions in the VPS13B (COH1) gene as a cause of Cohen syndrome. *Hum. Mutat.* 30:E845–E854. http://dx.doi.org/10.1002/humu.21065

Bankaitis, V.A., L.M. Johnson, and S.D. Emr. 1986. Isolation of yeast mutants defective in protein targeting to the vacuole. *Proc. Natl. Acad. Sci. USA.* 83:9075–9079. http://dx.doi.org/10.1073/pnas.83.23.9075

Bigay, J., and B. Antonny. 2005. Real-time assays for the assembly-disassembly cycle of COP coats on liposomes of defined size. *Methods Enzymol.* 404:95–107. http://dx.doi.org/10.1016/S0076-6879(05)04010-3

Blanchette, J.M., M.E. Abazeed, and R.S. Fuller. 2004. Cell-free reconstitution of transport from the *trans*-Golgi network to the late endosome/prevacuolar compartment. *J. Biol. Chem.* 279:48767–48773. http://dx.doi.org/10.1074/jbc.M406368200

Brachmann, C.B., A. Davies, G.J. Cost, E. Caputo, J. Li, P. Hieter, and J.D. Boeke. 1998. Designer deletion strains derived from *Saccharomyces cerevisiae* S288C: a useful set of strains and plasmids for PCR-mediated gene disruption and other applications. *Yeast.* 14:115–132. http://dx.doi.org/10.1002/(SICI)1097-0061(19980130)14:2<115::AID-YEA204>3.0.CO;2-2

Brenner, C., and R.S. Fuller. 1992. Structural and enzymatic characterization of a purified prohormone-processing enzyme: Secreted, soluble Kex2 protease. *Proc. Natl. Acad. Sci. USA.* 89:922–926. http://dx.doi.org/10.1073/pnas.89.3.922

Brickner, J.H., and R.S. Fuller. 1997. SOI1 encodes a novel, conserved protein that promotes TGN-endosomal cycling of Kex2p and other membrane proteins by modulating the function of two TGN localization signals. *J. Cell Biol.* 139:23–36. http://dx.doi.org/10.1083/jcb.139.1.23

Brickner, J.H., J.M. Blanchette, G. Sipos, and R.S. Fuller. 2001. The Tlg SNARE complex is required for TGN homotypic fusion. *J. Cell Biol.* 155:969–978. http://dx.doi.org/10.1083/jcb.200104093

Cooper, A.A., and T.H. Stevens. 1996. Vps10p cycles between the late-Golgi and prevacuolar compartments in its function as the sorting receptor for multiple yeast vacuolar hydrolases. *J. Cell Biol.* 133:529–541. http://dx.doi.org/10.1083/jcb.133.3.529

Cuff, J.A., M.E. Clamp, A.S. Siddiqui, M. Finlay, and G.J. Barton. 1998. JPred: a consensus secondary structure prediction server. *Bioinformatics.* 14:892–893. http://dx.doi.org/10.1093/bioinformatics/14.10.892

Danek, A., and R.H. Walker. 2005. Neuroacanthocytosis. *Curr. Opin. Neurol.* 18:386–392. http://dx.doi.org/10.1097/01.wco.0000173464.01888.e9

De, M., M.E. Abazeed, and R.S. Fuller. 2013. Direct binding of the Kex2p cytosolic tail to the VHS domain of yeast Gga2p facilitates TGN to prevacuolar compartment transport and is regulated by phosphorylation. *Mol. Biol. Cell.* 24:495–509. http://dx.doi.org/10.1091/mbc.E12-04-0322

Deloche, O., and R.W. Schekman. 2002. Vps10p cycles between the TGN and the late endosome via the plasma membrane in clathrin mutants. *Mol. Biol. Cell.* 13:4296–4307. http://dx.doi.org/10.1091/mbc.02-07-0105

Dobson-Stone, C., A. Danek, L. Rampoldi, R.J. Hardie, R.M. Chalmers, N.W. Wood, S. Bohlega, M.T. Dotti, A. Federico, M. Shizuka, et al. 2002. Mutational spectrum of the CHAC gene in patients with chorea-acanthocytosis. *Eur. J. Hum. Genet.* 10:773–781. http://dx.doi.org/10.1038/sj.ejhg.5200866

Frank, J., M. Radermacher, P. Penczek, J. Zhu, Y. Li, M. Ladjadj, and A. Leith. 1996. SPIDER and WEB: processing and visualization of images in 3D electron microscopy and related fields. *J. Struct. Biol.* 116:190–199. http://dx.doi.org/10.1006/jsbi.1996.0030

Grippa, A., L. Buxó, G. Mora, C. Funaya, F.Z. Idrissi, F. Mancuso, R. Gomez, J. Muntanyà, E. Sabidó, and P. Carvalho. 2015. The seipin complex Fld1/Ldb16 stabilizes ER-lipid droplet contact sites. *J. Cell Biol.* 211:829–844. http://dx.doi.org/10.1083/jcb.201502070

Gueldener, U., J. Heinisch, G.J. Koehler, D. Voss, and J.H. Hegemann. 2002. A second set of loxP marker cassettes for Cre-mediated multiple gene knockouts in budding yeast. *Nucleic Acids Res.* 30:e23. http://dx.doi.org/10.1093/nar/30.6.e23

Ivanovska, I., and M.D. Rose. 2001. Fine structure analysis of the yeast centrin, Cdc31p, identifies residues specific for cell morphology and spindle pole body duplication. *Genetics.* 157:503–518.

Kilmartin, J.V. 2003. Sfi1p has conserved centrin-binding sites and an essential function in budding yeast spindle pole body duplication. *J. Cell Biol.* 162:1211–1221. http://dx.doi.org/10.1083/jcb.200307064

Komano, H., and R.S. Fuller. 1995. Shared functions in vivo of a glycosyl-phosphatidylinositol-linked aspartyl protease, Mkc7, and the proprotein processing protease Kex2 in yeast. *Proc. Natl. Acad. Sci. USA.* 92:10752–10756. http://dx.doi.org/10.1073/pnas.92.23.10752

Krysan, D.J., E.L. Ting, C. Abeijon, L. Kroos, and R.S. Fuller. 2005. Yapsins are a family of aspartyl proteases required for cell wall integrity in *Saccharomyces cerevisiae*. *Eukaryot. Cell.* 4:1364–1374. http://dx.doi.org/10.1128/EC.4.8.1364-1374.2005

Lang, A.B., A.T. John Peter, P. Walter, and B. Kornmann. 2015. ER-mitochondrial junctions can be bypassed by dominant mutations in the endosomal protein Vps13. *J. Cell Biol.* 210:883–890. http://dx.doi.org/10.1083/jcb.201502105

Larkin, M.A., G. Blackshields, N.P. Brown, R. Chenna, P.A. McGettigan, H. McWilliam, F. Valentin, I.M. Wallace, A. Wilm, R. Lopez, et al. 2007. Clustal W and Clustal X version 2.0. *Bioinformatics.* 23:2947–2948. http://dx.doi.org/10.1093/bioinformatics/btm404

Lesage, S., V. Drouet, E. Majounie, V. Deramecourt, M. Jacoupy, A. Nicolas, F. Cormier-Dequaire, S.M. Hassoun, C. Pujol, S. Ciura, et al. International Parkinson's Disease Genomics Consortium (IPDGC). 2016. Loss of VPS13C function in autosomal-recessive Parkinsonism causes mitochondrial dysfunction and increases PINK1/Parkin-dependent mitophagy. *Am. J. Hum. Genet.* 98:500–513. http://dx.doi.org/10.1016/j.ajhg.2016.01.014

Li, S., A.M. Sandercock, P. Conduit, C.V. Robinson, R.L. Williams, and J.V. Kilmartin. 2006. Structural role of Sfi1p-centrin filaments in budding yeast spindle pole body duplication. *J. Cell Biol.* 173:867–877. http://dx.doi.org/10.1083/jcb.200603153

Marcusson, E.G., B.F. Horazdovsky, J.L. Cereghino, E. Gharakhanian, and S.D. Emr. 1994. The sorting receptor for yeast vacuolar carboxypeptidase Y is encoded by the VPS10 gene. *Cell.* 77:579–586. http://dx.doi.org/10.1016/0092-8674(94)90219-4

McCray, B.A., E. Skordalakes, and J.P. Taylor. 2010. Disease mutations in Rab7 result in unregulated nucleotide exchange and inappropriate activation. *Hum. Mol. Genet.* 19:1033–1047. http://dx.doi.org/10.1093/hmg/ddp567

Meda, S.A., B. Narayanan, J. Liu, N.I. Perrone-Bizzozero, M.C. Stevens, V.D. Calhoun, D.C. Glahn, L. Shen, S.L. Risacher, A.J. Saykin, and G.D. Pearlson. 2012. A large scale multivariate parallel ICA method reveals novel imaging-genetic relationships for Alzheimer's disease in the ADNI cohort. *Neuroimage.* 60:1608–1621. http://dx.doi.org/10.1016/j.neuroimage.2011.12.076

Miron, S., D. Durand, C. Chilom, J. Pérez, and C.T. Craescu. 2011. Binding of calcium, magnesium, and target peptides to Cdc31, the centrin of yeast *Saccharomyces cerevisiae*. *Biochemistry.* 50:6409–6422. http://dx.doi.org/10.1021/bi200518d

Downloaded from http://rupress.org/jcb/article-pdf/216/2/425/1597488/jcb_201606078.pdf by guest on 08 February 2026

Mumberg, D., R. Müller, and M. Funk. 1995. Yeast vectors for the controlled expression of heterologous proteins in different genetic backgrounds. *Gene.* 156:119–122. http://dx.doi.org/10.1016/0378-1119(95)00037-7

Muñoz-Braceras, S., R. Calvo, and R. Escalante. 2015. TipC and the chorea-acanthocytosis protein VPS13A regulate autophagy in *Dictyostelium* and human HeLa cells. *Autophagy.* 11:918–927. http://dx.doi.org/10.1080/15548627.2015.1034413

Ohi, M., Y. Li, Y. Cheng, and T. Walz. 2004. Negative staining and image classification: Powerful tools in modern electron microscopy. *Biol. Proced. Online.* 6:23–34. http://dx.doi.org/10.1251/bpo70

Otto, G.P., M. Razi, J. Morvan, F. Stenner, and S.A. Tooze. 2010. A novel syntaxin 6-interacting protein, SHIP164, regulates syntaxin 6-dependent sorting from early endosomes. *Traffic.* 11:688–705. http://dx.doi.org/10.1111/j.1600-0854.2010.01049.x

Park, J.S., and A.M. Neiman. 2012. VPS13 regulates membrane morphogenesis during sporulation in *Saccharomyces cerevisiae*. *J. Cell Sci.* 125:3004–3011. http://dx.doi.org/10.1242/jcs.105114

Park, J.S., Y. Okumura, H. Tachikawa, and A.M. Neiman. 2013. SPO71 encodes a developmental stage-specific partner for Vps13 in *Saccharomyces cerevisiae*. *Eukaryot. Cell.* 12:1530–1537. http://dx.doi.org/10.1128/EC.00239-13

Park, J.S., S. Halegoua, S. Kishida, and A.M. Neiman. 2015. A conserved function in phosphatidylinositol metabolism for mammalian Vps13 family proteins. *PLoS One.* 10:e0124836. http://dx.doi.org/10.1371/journal.pone.0124836

Park, J.S., M.K. Thorsness, R. Policastro, L.L. McGoldrick, N.M. Hollingsworth, P.E. Thorsness, and A.M. Neiman. 2016. Yeast Vps13 promotes mitochondrial function and is localized at membrane contact sites. *Mol. Biol. Cell.* 27:2435–2449. http://dx.doi.org/10.1091/mbc.E16-02-0112

Petracek, M.E., and M.S. Longtine. 2002. PCR-based engineering of yeast genome. *Methods Enzymol.* 350:445–469. http://dx.doi.org/10.1016/S0076-6879(02)50978-2

Pfisterer, S.G., D. Bakula, T. Frickey, A. Cezanne, D. Brigger, M.P. Tschan, H. Robenek, and T. Proikas-Cezanne. 2014. Lipid droplet and early autophagosomal membrane targeting of Atg2A and Atg14L in human tumor cells. *J. Lipid Res.* 55:1267–1278. http://dx.doi.org/10.1194/jlr.M046359

Redding, K., M. Seeger, G.S. Payne, and R.S. Fuller. 1996. The effects of clathrin inactivation on localization of Kex2 protease are independent of the TGN localization signal in the cytosolic tail of Kex2p. *Mol. Biol. Cell.* 7:1667–1677. http://dx.doi.org/10.1091/mbc.7.11.1667

Rose, M.D., F. Winston, and P. Hieter. 1990. Methods in Yeast Genetics: A Laboratory Course Manual. Cold Spring Harbor Laboratory, Cold Spring Harbor, NY. 198 pp.

Salisbury, J.L. 2004. Centrosomes: Sfi1p and centrin unravel a structural riddle. *Curr. Biol.* 14:R27–R29. http://dx.doi.org/10.1016/j.cub.2003.12.019

Samaranayake, H.S., A.E. Cowan, and L.A. Klobutcher. 2011. Vacuolar protein sorting protein 13A, TtVPS13A, localizes to the *Tetrahymena thermophila* phagosome membrane and is required for efficient phagocytosis. *Eukaryot. Cell.* 10:1207–1218. http://dx.doi.org/10.1128/EC.05089-11

Scheres, S.H. 2012. RELION: implementation of a Bayesian approach to cryo-EM structure determination. *J. Struct. Biol.* 180:519–530. http://dx.doi.org/10.1016/j.jsb.2012.09.006

Seifert, W., M. Holder-Espinasse, J. Kühnisch, K. Kahrizi, A. Tzschach, M. Garshasbi, H. Najmabadi, A. Walter Kuss, W. Kress, G. Laureys, et al. 2009. Expanded mutational spectrum in Cohen syndrome, tissue expression, and transcript variants of COH1. *Hum. Mutat.* 30:E404–E420. http://dx.doi.org/10.1002/humu.20886

Seifert, W., J. Kühnisch, T. Maritzen, D. Horn, V. Haucke, and H.C. Hennies. 2011. Cohen syndrome-associated protein, COH1, is a novel, giant Golgi matrix protein required for Golgi integrity. *J. Biol. Chem.* 286:37665–37675. http://dx.doi.org/10.1074/jbc.M111.267971

Seifert, W., J. Kühnisch, T. Maritzen, S. Lommatzsch, H.C. Hennies, S. Bachmann, D. Horn, and V. Haucke. 2015. Cohen syndrome-associated protein COH1 physically and functionally interacts with the small GTPase RAB6 at the Golgi complex and directs neurite outgrowth. *J. Biol. Chem.* 290:3349–3358. http://dx.doi.org/10.1074/jbc.M114.608174

Shiokawa, N., M. Nakamura, M. Sameshima, A. Deguchi, T. Hayashi, N. Sasaki, and A. Sano. 2013. Chorein, the protein responsible for chorea-acanthocytosis, interacts with β-adducin and β-actin. *Biochem. Biophys. Res. Commun.* 441:96–101. http://dx.doi.org/10.1016/j.bbrc.2013.10.011

Sipos, G., J.H. Brickner, E.J. Brace, L. Chen, A. Rambourg, F. Kepes, and R.S. Fuller. 2004. Soi3p/Rav1p functions at the early endosome to regulate endocytic trafficking to the vacuole and localization of trans-Golgi network transmembrane proteins. *Mol. Biol. Cell.* 15:3196–3209. http://dx.doi.org/10.1091/mbc.E03-10-0755

Stols, L., M. Gu, L. Dieckman, R. Raffen, F.R. Collart, and M.I. Donnelly. 2002. A new vector for high-throughput, ligation-independent cloning encoding a tobacco etch virus protease cleavage site. *Protein Expr. Purif.* 25:8–15. http://dx.doi.org/10.1006/prep.2001.1603

Strawbridge, R.J., J. Dupuis, I. Prokopenko, A. Barker, E. Ahlqvist, D. Rybin, J.R. Petrie, M.E. Travers, N. Bouatia-Naji, A.S. Dimas, et al. C4D Consortium. 2011. Genome-wide association identifies nine common variants associated with fasting proinsulin levels and provides new insights into the pathophysiology of type 2 diabetes. *Diabetes.* 60:2624–2634. http://dx.doi.org/10.2337/db11-0415

Trybus, K.M., M.I. Gushchin, H. Lui, L. Hazelwood, E.B. Krementsova, N. Volkmann, and D. Hanein. 2007. Effect of calcium on calmodulin bound to the IQ motifs of myosin V. *J. Biol. Chem.* 282:23316–23325. http://dx.doi.org/10.1074/jbc.M701636200

Velayos-Baeza, A., A. Vettori, R.R. Copley, C. Dobson-Stone, and A.P. Monaco. 2004. Analysis of the human VPS13 gene family. *Genomics.* 84:536–549. http://dx.doi.org/10.1016/j.ygeno.2004.04.012

Wilcox, C.A., and R.S. Fuller. 1991. Posttranslational processing of the prohormone-cleaving Kex2 protease in the *Saccharomyces cerevisiae* secretory pathway. *J. Cell Biol.* 115:297–307. http://dx.doi.org/10.1083/jcb.115.2.297

Wilcox, C.A., K. Redding, R. Wright, and R.S. Fuller. 1992. Mutation of a tyrosine localization signal in the cytosolic tail of yeast Kex2 protease disrupts Golgi retention and results in default transport to the vacuole. *Mol. Biol. Cell.* 3:1353–1371. http://dx.doi.org/10.1091/mbc.3.12.1353

Yang, Z., J. Fang, J. Chittuluru, F.J. Asturias, and P.A. Penczek. 2012. Iterative stable alignment and clustering of 2D transmission electron microscope images. *Structure.* 20:237–247. http://dx.doi.org/10.1016/j.str.2011.12.007

Downloaded from http://rupress.org/jcb/article-pdf/216/2/425/1597488/jcb_201606078.pdf by guest on 08 February 2026